

3-D Symmetry Detection and Analysis Using the Pseudo-polar Fourier Transform

Amit Bermanis · Amir Averbuch · Yosi Keller

Received: 15 November 2007 / Accepted: 13 May 2010 / Published online: 26 May 2010
© Springer Science+Business Media, LLC 2010

Abstract Symmetry detection and analysis in 3D images is a fundamental task in a gamut of scientific fields such as computer vision, medical imaging and pattern recognition to name a few. In this work, we present a computational approach to 3D symmetry detection and analysis. Our analysis is conducted in the Fourier domain using the pseudo-polar Fourier transform. The pseudo-polar representation enables to efficiently and accurately analyze angular volumetric properties such as rotational symmetries. Our algorithm is based on the analysis of the angular correspondence rate of the given volume and its rotated and rotated-inverted replicas in their pseudo-polar representations. We also derive a novel rigorous analysis of the inherent constraints of 3D symmetries via groups-theory based analysis. Thus, our algorithm starts by detecting the rotational symmetry group of a given volume, and the rigorous analysis results pave the way to detect the rest of the symmetries. The complexity of the algorithm is $O(N^3 \log(N))$, where $N \times N \times N$ is the volumetric size in each direction. This complexity is independent of the number of the detected symmetries. We experimentally verified our approach by applying it to synthetic as well as real 3D objects.

Keywords 3D symmetry · Pseudo-polar · Symmetry groups

A. Bermanis · A. Averbuch (✉)
School of Mathematical Sciences, Tel Aviv University,
Tel-Aviv 69978, Israel
e-mail: amir@math.tau.ac.il

A. Bermanis
e-mail: amitberm@post.tau.ac.il

Y. Keller
School of Engineering, Bar Ilan University, Ramat-Gan, Israel
e-mail: yosi.keller@gmail.com

1 Introduction

A multitude of objects around us exhibit some form of symmetry. Much of human perception and sense of aesthetics is based on recognition of symmetric patterns (Thompson 1961). Moreover, many man-made objects such as airplanes and houses and natural objects such as insects and molecules (see Fig. 1) exhibit some form of symmetry, making symmetry an efficient visual cue for detecting objects of interest.

Hence, symmetry detection has become a fundamental task in computer vision and has attracted significant research efforts (Cornelius et al. 2007; Derrode and Ghorbel 2004; Kazhdan et al. 2002; Kiryati and Gofman 1998; Loy and Eklundh 2006; Lucchese 2004; Reisfeld et al. 1995; Shen et al. 2001; Prasad and Davis 2005). Most of these works deal with the analysis of two-dimensional symmetries (rather than 3D symmetries) as the acquisition of images is a ubiquitous application and easier to handle both algorithmically and computationally. Recently, with the advance in 3D acquisition devices, the analysis of 3D geometry in general and symmetry of particular has gain a growing interest (Kazhdan et al. 2002; Pauly et al. 2008; Mitra et al. 2006). Symmetry analysis algorithms can be categorized as either being feature or intensity-based, where feature based representations refer to 2D/3D objects given by points clouds or meshes (graphs). In contrast, intensity based approaches are applicable when the object of interest is given by a discrete function, such as image or a volume.

A 2D object is said to have rotational symmetry of order K if it is invariant under $\frac{2\pi}{K}k$, $k = 0, \dots, K - 1$, rotations of about a point denoted as the *symmetry center*. Whereas an object has reflectional symmetry if it is invariant under a reflection transformation about a line, denoted the *reflection axis*. However, this formulation does not carry over to 3D objects. Consider for instance Fig. 1d where one of the rotational symmetries is given about a vertical axis rather than

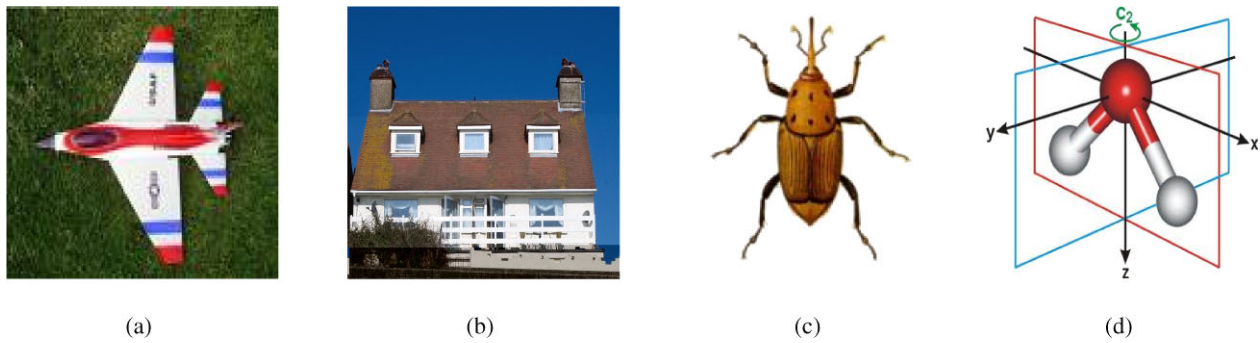


Fig. 1 Symmetric objects. (a) Airplane—reflective symmetry in respect to the horizontal plane. (b) House. (c) Insect—reflective symmetry in respect to the vertical plane. (d) H₂O molecule—reflective

symmetries in respect to the x - z and y - z planes and rotational symmetry in respect to z -axis

a symmetry center as in the 2D case. Moreover, 2D symmetry was shown to be a constrained phenomenon, where given a subset of the symmetry's reflections or rotations one can analytically deduce the overall set of symmetry transformations. A comprehensive review of these properties for the 2D case was given by Chertok and Keller (2009).

In this work we study the symmetries of 3D volumes. The term *volume* refers to a 3D image V that is given on a 3D Cartesian grid. Our goal is to detect all the isometries $T: \mathbb{R}^3 \rightarrow \mathbb{R}^3$, s.t. V is invariant under their action. The symmetry groups that we explore are finite and according to the boundness of the volumes. For instance, the molecule in Fig. 1d is invariant to its rotation by π radians about the z -axis and also by reflecting it in respect to the x - z and y - z planes. Therefore, in addition to the identity transformation, these transformations constitute the symmetry group of the molecule. As 3D symmetry is a polar property. Therefore, we propose to use of the pseudo-polar Fourier representation (Averbuch and Shkolnisky 2003) that was shown to be an efficient computational tool for the analysis of polar properties in applications such as 2D symmetry analysis (Keller and Shkolnisky 2006), image registration (Keller et al. 2005a, 2005b), and volume registration (Keller et al. 2006). Most of the recent work on 3D symmetry, in the computer graphics community in particular, is based on the analysis of mesh based representations (Kazhdan et al. 2002; Pauly et al. 2008; Mitra et al. 2006; Bronstein et al. 2009), while the analysis of volume data is scarce although such data sources (MRI, CT) are common.

In this work we propose two contributions:

First, we present a novel rigorous analysis of the inherent constraints between 3D symmetry transformations via group theory analysis. This is the 3D equivalent of the 2D case mentioned above (Chertok and Keller 2009). But in contrast to the 2D, the constraints cannot be derived by straight forward trigonometric computations. Thus, we apply group-theory analysis to

derive the constraints between the rotations group of a volume and its opposite symmetries.

Second, we present a new computational approach to symmetry detection of 3D volumes using the 3D Pseudo-Polar Fourier Transform (3DPPFT) (Averbuch and Shkolnisky 2003) and the Angular Difference Function (ADF). The ADF was introduced by Keller et al. (2006) and applied to volume registration. It measures the correspondence between two volumes along rays in the same direction. Thus, it allows to formulate the symmetry analysis problem in terms of volume self-registration. The algorithm detects both perfect and imperfect symmetries, by first detecting the rotational symmetry group of the given volume. This group enables to detect the reflective symmetries using the results of our rigorous analysis. The computational complexity of the scheme is $O(N^3 \log(N))$, where $N \times N \times N$ are the volume's dimensions, and it is invariant to the number of symmetries.

The paper is organized as follows: Sect. 2 presents previous results on 3D symmetry detection and analysis. Section 3 provides the mathematical formulation of symmetries as well as the angular properties of the Fourier domain and the ADF. Section 4 presents the 3D Symmetry Detection Algorithm (3DSDA), which is experimentally verified in Sect. 5 by applying it to real as well as synthetic volumes that contain both perfect and imperfect symmetries.

2 Related Work

Symmetry has been thoroughly studied in previous works, where the body of work was conducted on 2D symmetry analysis. Although this work deals with volumes analysis, we survey 2D solutions as well since these provide useful intuitions and emphasize the inherent difficulties in 3D analysis.

Theoretical analysis of 2D symmetries can be found in Miller (1972), Weyl (1952). One of the earliest approaches to intensity based symmetry analysis is the use of numerical polar moments of images and image patches. One-dimensional odd-even decompositions were used by Chen (2001) to detect vertical symmetry axes, while Kim and Kim (1999) utilizes the Zernike moments to estimate the relative rotations between patterns and thus recover the symmetries. The Zernike moments of two rotated images will have the same magnitude and some phase differential, where the phase differential can be used to estimate the relative rotation. Unfortunately, in order to detect large symmetric objects, such schemes require an exhaustive search over all the potential symmetry axes and locations in the image. This requires excessive computations even for small images and thus, can not be extended to 3D volumes.

Kiryati and Gofman (1998) proposed to resolve the computational complexity issue by deriving an efficient genetic search algorithm that maximizes a local symmetry detector over the set of four parameters x , y , θ , and r , where x and y are the center of the examined area, r is its radius and θ is the angle of the reflection axis.

Recent work emphasizes the use of *local* image features. The local information is then agglomerated to detect the global symmetry. Reisfeld et al. (1995) suggested a low-level operator for interest points detection where symmetry is considered a cue. This symmetry operator constructs the symmetry map of the image by computing an edge map, where the magnitude and orientation of each edge depend on the symmetry associated with each of its pixels. The proposed operator is able to process different symmetry scales, enabling it to be used in multi-resolution schemes.

The gradient vector flow field was used in Prasad and Yegnanarayana (2004) to compute a local feature vector. For each point, its location, orientation and magnitude were retained. Local features in the form of Taylor coefficients of the field were computed and a hashing algorithm is then applied to detect pairs of points with symmetric fields, while a voting scheme is used to robustly identify the location of symmetry axis.

SIFT local image features (Lowe 2003) were applied to symmetry analysis by Loy and Eklundh (2006). In their scheme, a set of feature points is detected over the image and the corresponding SIFT descriptors are computed. Feature points are then matched in pairs by the similarity of their SIFT descriptors. These local pairwise symmetries are then agglomerated by a Hough voting space of symmetry axes. The vote of each pair in the Hough domain is given by a weight function that measures the discrepancy in the dominant angles and scales (Lowe 2003) of the feature points.

Several authors proposed to extend the SIFT local features to high-dimensional data (Ni et al. 2009; Cheung and Hamarneh 2007). These were applied to the mosaicing 3D

medical scans. But, such schemes were found to be difficult to extend to 3D data due to the increased dimensionality of the symmetry parameters, resulting in an exponential increase in the computational complexity.

Fourier domain based approaches are of particular interest to us as they relate to our proposed scheme. In particular, Fourier based analysis of 3D data is a well founded computational technique both for Cartesian as well as polar domains (Averbuch and Shkolnisky 2003). The unitarity of the Fourier transform preserves the symmetry of images in the Fourier domain: a symmetric object in the intensity domain will also be symmetric in the Fourier domain. Furthermore, the phase-shift property of the Fourier domain allows to compute shift-invariant representations of 2D/3D functions. Thus, the estimation of the rotational symmetry attributes (rotations, reflections) can be decoupled from the computation of the related translations. Lucchese (2004) provides an elegant approach to analyze the angular properties of an image without computing its polar DFT. An angular histogram is computed by detecting and binning the pointwise zero crossings of the difference of the Fourier magnitude in Cartesian coordinates along rays. The histogram's maxima correspond to the direction of the zero crossing. Keller and Shkolnisky (2006) extended Lucchese's work, by applying the PseudoPolar Fourier transform to computing algebraically-accurate line integral in the Fourier domain. The symmetry resulted in a periodic pattern in the line integral result. The registration of 3D data using the 3DPPFT was studied by Keller et al. (2006), where they proposed a 3D variant of the Angular Difference Function (ADF) as an efficient mean for analyzing 3D rotations. In this work we propose to consider symmetry as a particular case of self-alignment and show how to utilize the computational efficiency of the ADF approach.

Fourier analysis on a sphere, namely spherical harmonics, was suggested by Kazhdan et al. (2002) who proposed to compute a reflectional symmetry descriptor that measures the amount of reflectional symmetry of 3D volumes for all planes through the center of mass. This descriptor maps any 3D volume to a sphere, where each point on the sphere represents the amount of symmetry in the object with respect to the plane perpendicular to the direction of the point. As each point on the sphere also represents the integration over the entire volume, the descriptor was shown to be resilient to noise and to small variations between objects. A related approach was proposed by Martinet et al. (2006). They propose to compute the generalized even moments and expand it over a sphere using spherical harmonic, which are shown to encode the parameters of the symmetries of the shape.

The body of recent works in 3D symmetry analysis stems from the computer graphics community and aims at analyzing mesh objects and clouds of 3D points. An agglomerative approach to the detection of reflectional symmetries of

mesh objects was proposed by Mitra et al. (2006). They detect local reflectional symmetries by computing local signatures that are based on curvature and on the normal's direction at each point. The signatures are matched and for each such match, the symmetry parameters are encoded in a feature space. The dominant symmetries are detected in the feature space using mean-shift clustering. Bokeloh et al. (2009) proposed a similar clustering based approach for symmetry detection in clouds of points. First, they detect lines in the model of interest that are locally clustered into graphs of local features denoted as *bases*. RANSAC is then used to find similar bases in the set of points. Once the symmetry is detected, the authors proposed to utilize them for holes filling and the reconstruction of missing data section within the set of points.

A different type of 3D symmetry is commonly known as *translational symmetry*. The term refers to the detection of near-regular patterns, where the repetition might be either angular or translational. In images, translational symmetry is manifested by texture and lattices and was studied by Hays et al. (2006) by combining the use of local image descriptors and spectral high-order assignments. Pauly et al. (2008) studied the detection of translational symmetry in mesh objects by extending the work of Mitra et al. (2006). They limit the feature space used in Mitra et al. (2006) to scale, rotations and translations. The identified repeated patches are utilized to reconstruct data from scattered point samples.

Ovsjanikov et al. (2008) derived a spectral embedding based approach to detect reflectional symmetries in meshes. They show that in the diffusion coordinates given by the eigenfunctions of the Laplace-Beltrami operator, reflectional intrinsic non-rigid symmetries are transformed into Euclidean ones and can thus be efficiently detected. Raviv et al. (2007) analyzed symmetries of non-rigid 3D shapes by formulating them as an intrinsic self-similarity. The intrinsic similarity between non-rigid shapes was estimated using a method based on geodesic distances and self-registering the volumes using a method proposed by Bronstein et al. (2006).

3 Mathematical Preliminaries

In this section, we present the mathematical tools and concepts used in deriving the proposed scheme in general and algorithms 1–7 (Sect. 4), in particular. We start by presenting the relevant properties of finite symmetries groups in \mathbb{R}^3 and the relations between two types of symmetries: rotations and rotation-inversions. In addition, we describe the Pseudo-Polar Fourier transform and the Angular Difference Function (ADF) that play a central role in the numerical implementation of our symmetry analysis algorithms.

3.1 Isometries in \mathbb{R}^3

Any symmetry in \mathbb{R}^3 can be represented by an orthogonal 3×3 matrix. The set of 3D isometries constitutes a group that is denoted by $\mathcal{O}(3)$ (the orthogonal group). Any element $O \in \mathcal{O}^3$ preserves the geometry in \mathbb{R}^3 i.e., preserves the standard inner product $\langle \cdot, \cdot \rangle$. Its representative matrix determinant is either 1 or -1 and its inverse is equal to its conjugate. O denotes a **rotation** if $\det(O) = 1$, otherwise, O denotes a **rotation-inversion**.

3.1.1 Rotations

The subgroup of all the rotations in $\mathcal{O}(3)$ is called the **special orthogonal group in \mathbb{R}^3** denoted by $\mathcal{SO}(3)$. Any rotation O is given by its rotation axis and by its rotation angle. The rotation axis is an eigenvector $\vec{f} = (f_1 \ f_2 \ f_3)^T$ of O corresponding to the eigenvalue 1. The rotation angle γ is the angle between \vec{x} and $O\vec{x}$, for any vector \vec{x} which is perpendicular to \vec{f} (Miller 1972). \vec{f} is given by the two spherical angles θ and ϕ , s.t.

$$f_1 = \sin \phi \cos \theta, \quad f_2 = \sin \phi \sin \theta, \quad f_3 = \cos \phi,$$

where $0 \leq \theta < 2\pi$ and $0 \leq \phi < \pi$. According to Euler's rotation theorem (Trucco and Verri 1998), the rotation matrix O is

$$O = E \cos \gamma + (1 - \cos \gamma) \begin{pmatrix} f_1^2 & f_1 f_2 & f_1 f_3 \\ f_1 f_2 & f_2^2 & f_2 f_3 \\ f_1 f_3 & f_2 f_3 & f_3^2 \end{pmatrix} + \sin \gamma \begin{pmatrix} 0 & -f_3 & f_2 \\ f_3 & 0 & -f_1 \\ -f_2 & f_1 & 0 \end{pmatrix}, \quad (3.1)$$

where E is the 3×3 identity matrix. If $\gamma = \frac{2\pi}{n}$, $n \in \mathbb{N}$, then, O denotes a **rotation of order n** .

3.1.2 Rotation-inversions

Let R be a rotation-inversion, then, $O_R \triangleq -R$ is a rotation. Hence, any rotation-inversion R can be written as $R = -O_R$ and R has an eigenvalue of -1 . Two important examples of rotation-inversions are reflection and inversion. Since these transformations play a vital role in symmetry analysis they are further discussed.

Reflection is a rotation-inversion that has two eigenvalues 1 and -1 . The eigenspace, which corresponds to the eigenvalue 1, is called the **reflection plane of R** , and the eigenvector, which corresponds to the eigenvalue -1 , is called the **reflection axis of R** . The reflection plane is perpendicular to

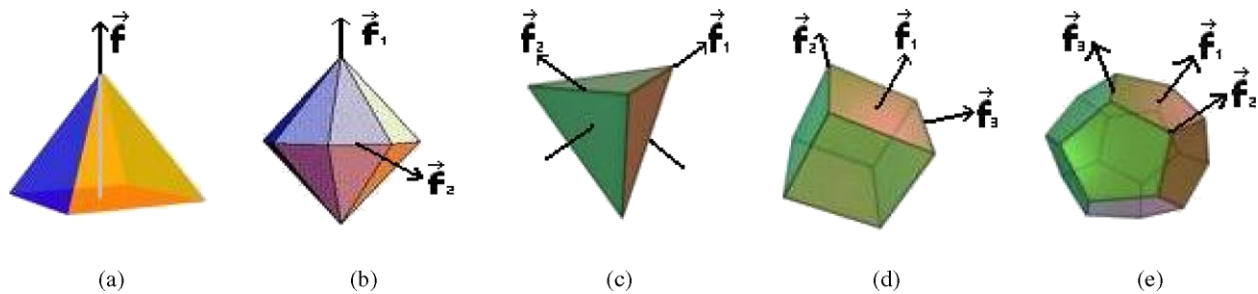


Fig. 2 Symmetric volumes with nontrivial rotations groups. (a) Cyclic rotations group. \vec{f} is a single fourfold rotation axis. (b) Dihedric rotations group. \vec{f}_1 is the principal sixfold rotation axis and \vec{f}_2 is one of six twofold rotation axes. (c) Tetrahedric rotations group. \vec{f}_1 is one of four threefold axes and \vec{f}_2 is one of three twofold axes. (d) Octahedric rotations group. \vec{f}_1 is one of three fourfold axes, \vec{f}_2 is one of four threefold axes and \vec{f}_3 is one of six twofold axes. (e) Icosahedric rotations group. \vec{f}_1 is one of six fivefold axes, \vec{f}_2 is one of ten threefold axes and \vec{f}_3 is one of fifteen twofold axes

the reflection axis, and the reflection operator, whose axis is \vec{f} , is given by Eckmann Jeger and Jeger (1967) as

$$R_{\vec{f}}(\vec{x}) = \vec{x} - 2 \frac{\langle \vec{x}, \vec{f} \rangle}{\|\vec{f}\|^2} \vec{f}.$$

Any reflection R satisfies $R = R^{-1}$ or, equivalently, R is self conjugate.

Inversion, denoted by I , is the linear transformation $I(\vec{x}) = -\vec{x}$.

The only rotation-inversion of order two is either reflection or inversion.

3.2 Symmetric Volumes

In this section, we classify the symmetries of volumes, whose rotations groups are finite and nontrivial, into five classes. We derive the relationships and the inner-constraints between the rotation groups of a volume and the rest of its symmetry group. Denote by $\Lambda(T)V$ the action of T on a volume V . We have

$$\Lambda(T)V(\vec{x}) \triangleq V(T^{-1}\vec{x}), \quad \vec{x} \in \mathbb{R}^3. \quad (3.2)$$

Definition 3.1 Let V be a volume. $O \in \mathcal{O}(3)$ is called a **symmetry of V** if $\Lambda(O)V = V$.

The **symmetry group of V** , denoted by \mathcal{G}_V , is the group of all symmetries of V , whose operation is defined by (3.2). Since $E \in \mathcal{G}_V$ for any volume V , $\mathcal{G}_V \neq \emptyset$. The subgroup of \mathcal{G}_V , which contains only rotations, is called the **rotations group of V** , denoted by \mathcal{K}_V . We are interested only in volumes whose symmetry groups are finite, unlike a ball, for instance, whose symmetry group is $\mathcal{O}(3)$.

V is a **symmetric volume** if $\mathcal{G}_V \neq \{E\}$. A vector $\vec{f} \in \mathbb{R}^3$ is called a **rotation axis of V** if there is a rotation $O \in \mathcal{K}_V$ whose rotation axis is \vec{f} . If \vec{f} is a rotation axis of V , then, there is a rotation $O \in \mathcal{K}_V$ of maximal order $n \in \mathbb{N}$, whose

axis is \vec{f} , i.e. there are n rotations in \mathcal{K}_V , which are associated with \vec{f} . The subgroup of these rotations is the **cyclic group**, whose **generator** is O , i.e., $\langle O \rangle \triangleq \{O^k : k = 1, 2, \dots, n-1\}$. In this case, \vec{f} is called **n -fold rotation axis of V** . \mathcal{P} is called **reflection plane of V** and \vec{f} is called **reflection axis of V** if there is a reflection $R \in \mathcal{G}_V$, s.t., \mathcal{P} and \vec{f} are its reflection plane and reflection axis, respectively. If \mathcal{G} is a subgroup of $\mathcal{O}(3)$ and \mathcal{K} is its rotations subgroup, then, either $\mathcal{G} = \mathcal{K}$ or $\mathcal{G} = \mathcal{K} \cup R\mathcal{K}$, where R is a rotation-inversion of order two (Miller 1972). Hence, R is either a reflection or an inversion.

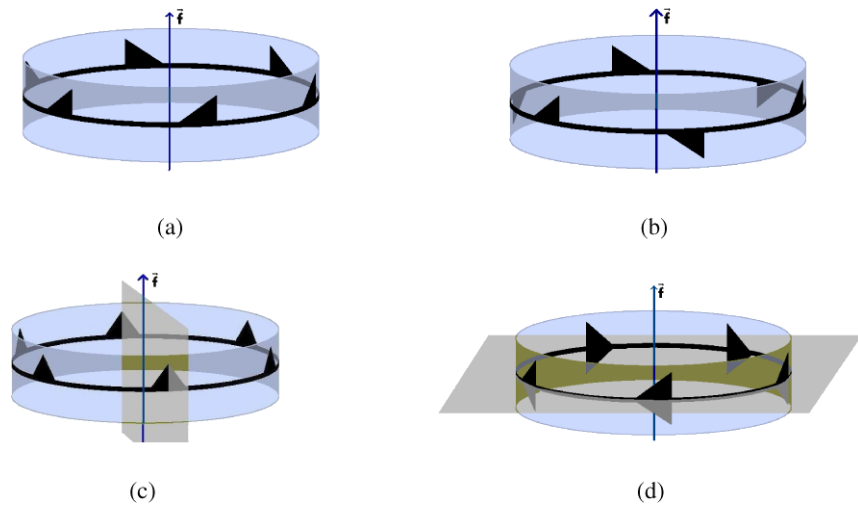
The finite non-trivial subgroups of $\mathcal{SO}(3)$ can be classified into five categories:

1. **Cyclic:** \mathcal{K}_V is a cyclic group of order n , $n > 1$. In this case, V has exactly one n -fold rotation axis, see Fig. 2(a).
2. **Dihedric:** $|\mathcal{K}_V| = 2m$, $m \geq 2$. In this case, V has one m -fold rotation axis, which is called the **principal axis of V** , and m twofold rotation axes, which are called the **secondary rotation axes of V** . The secondary rotation axes are all perpendicular to the principal axis. The angle between any two adjacent axes of these twofold axes is $\frac{\pi}{m}$, see Fig. 2(b).
3. **Tetrahedric:** $|\mathcal{K}_V| = 12$. V has four threefold rotation axes and three twofold rotation axes, see Fig. 2(c).
4. **Octahedric:** $|\mathcal{K}_V| = 24$. V has three fourfold rotation axes, four threefold rotation axes and six twofold rotation axes, see Fig. 2(d).
5. **Icosahedric:** $|\mathcal{K}_V| = 60$. V has six fivefold rotation axes, ten threefold rotation axes and fifteen twofold rotation axes, see Fig. 2(e).

Our next goal is to associate a detected rotation-inversion transform with its corresponding subgroup of rotations for a given volume. If $I \notin \mathcal{G}_V$, then, \mathcal{K}_V is either Cyclic, Dihedric or Tetrahedric (Stoy et al. 1994).

Fig. 3 Cyclic rotations groups.

(a) $\mathcal{G}_V = \mathcal{K}_V$ is cyclic of order six with a rotation axis \vec{f} .
 (b) \mathcal{K}_V is cyclic of order three, $I \in \mathcal{G}_V$. (c) \mathcal{K}_V is cyclic of order six, $R \in \mathcal{G}_V$ is a reflection that satisfies $R\vec{f} = \vec{f}$. (d) \mathcal{K}_V is cyclic of order five, $R \in \mathcal{G}_V$ is a reflection which satisfies $R\vec{f} = -\vec{f}$.



3.2.1 Cyclic Rotations Subgroup

Lemma 3.1 Let $\mathcal{K}_V = \langle O \rangle$ be a cyclic group of order $n > 1$, $\mathcal{G}_V \neq \mathcal{K}_V$ and $I \notin \mathcal{G}_V$. Then, there is a reflection $R \in \mathcal{G}_V$, which either satisfies $R\vec{f} = \vec{f}$ or $R\vec{f} = -\vec{f}$, where \vec{f} is the rotation axis of O (see Figs. 3(c) and 3(d)). Moreover, if $R\vec{f} = \vec{f}$, then, all the rotation-inversions in \mathcal{G}_V RO^k , $k = 0, 1, \dots, n-1$ are reflections.

Proof Since $\mathcal{G}_V \neq \mathcal{K}_V$ and $I \notin \mathcal{G}_V$, there is a reflection $R \in \mathcal{G}_V$. $ROR \in \mathcal{K}_V$, i.e., there is $j \in \mathbb{N}$, s.t. $ROR = O^j$. As a consequence, $OR\vec{f} = R\vec{f}$. Hence, either $R\vec{f} = \vec{f}$ or $R\vec{f} = -\vec{f}$. If $R\vec{f} = \vec{f}$, then, $RO^k\vec{f} = \vec{f}$ i.e. RO^k is rotation-inversion with eigenvalue 1, hence, RO^k is a reflection for any $k = 0, 1, \dots, n-1$. \square

Following Lemma 3.1, if $I \notin \mathcal{G}_V$ and $R\vec{f} \notin \mathcal{G}_V$, then any rotation-inversion in \mathcal{G}_V is a reflection. This will be used in Sect. 4.3, where we recover the reflection parameters of a cyclic volume.

3.2.2 Dihedric Rotations Subgroup

Lemma 3.2 Let V be a Dihedron, $\mathcal{G}_V \neq \mathcal{K}_V$ and $I \notin \mathcal{K}_V$. Then, there is a reflection $\tilde{R} \in \mathcal{G}_V$, which satisfies $\tilde{R}\vec{f} = \vec{f}$, where \vec{f} is the principal axis of V .

Proof Let $R \in \mathcal{G}_V$ be a reflection and $O \in \mathcal{K}_V$ be the rotation associated with \vec{f} . As $ROR \in \mathcal{K}_V$, either $ROR = O^k$, $k \in \mathbb{Z}$, or $ROR = O_j$, where $O_j \in \mathcal{K}_V$ is a secondary rotation. By considering the first possibility, we get $OR\vec{f} = R\vec{f}$, i.e. either $R\vec{f} = \vec{f}$ or $R\vec{f} = -\vec{f}$. If $R\vec{f} = \vec{f}$, then, $\tilde{R} = R$. Otherwise, $R\vec{f} = -\vec{f}$. Let $O_j \in \mathcal{K}_V$ be a secondary rotation and let $\tilde{R} \triangleq O_j R$. Then, $\tilde{R} \in \mathcal{G}_V$ is a rotation-inversion, which satisfies $\tilde{R}\vec{f} = \vec{f}$, i.e., \tilde{R} is reflection, which satisfies the required. By considering the sec-

ond possibility, we get $ROR\vec{f} = O_j\vec{f} = -\vec{f}$, or equivalently, $OR\vec{f} = -R\vec{f}$, i.e. O has eigenvalue -1 , hence, O is of order two. Then, $\{\vec{f}, \vec{f}_1, \vec{f}_2\}$ is an orthogonal set, where \vec{f}_1 and \vec{f}_2 are the two additional rotation axes of V . Without loss of generality, assume that $ROR = O_1$, where O_1 is the secondary rotation associated with \vec{f}_1 . In this case, $OR\vec{f}_1 = R\vec{f}_1$, i.e. $R\vec{f}_1 = \pm\vec{f}$ and $R\vec{f}_2 = \vec{f}_2$. If $ROR = O_1$ is assumed, we get $R\vec{f}_1 = \vec{f}_1$. \square

If \vec{f} is a twofold rotation axis of V , then, each of the rotation axes can be considered as the principal axis. Let \vec{f}_0 be one of the secondary rotation axes of a Dihedron. The rest of the secondary rotation axes can be enumerated according to the rule $\vec{f}_j \triangleq O^j \vec{f}_0$, $j = 1, \dots, m-1$, and $\angle(\vec{f}_i, \vec{f}_k) = \pi \frac{|l-k|}{m}$.

Lemma 3.3 Let V be a Dihedron, whose principal axis is \vec{f} , $\mathcal{G}_V \neq \mathcal{K}_V$ and $I \notin \mathcal{K}_V$. Then, there is a reflection $R \in \mathcal{G}_V$, which satisfies $R\vec{f} = \vec{f}$ and $R\vec{v} = \vec{v}$, where $\vec{v} \in \mathbb{R}^3$ is an angle bisector between two adjacent secondary rotation axes of V .

Proof From Lemma 3.2, it follows that there is a reflection $R \in \mathcal{G}_V$, which satisfies $R\vec{f} = \vec{f}$. Let $\vec{v} \in \mathbb{R}^3$ be a vector, which satisfies $\vec{v} \perp \vec{f}$ and $R\vec{v} = \vec{v}$. Then, $\vec{v} \in \text{span}\{\vec{f}_j\}_{j=0}^{m-1}$, where $\{\vec{f}_j\}_{j=0}^{m-1}$ are the secondary rotation axes of V and m is the order of the principal rotation O . Assume that \vec{v} is not one of the secondary rotation axes and let \vec{f}_k be the secondary rotation axis, which satisfies $\angle(\vec{v}, \vec{f}_k) = \min_{j=0, \dots, m-1} \angle(\vec{v}, \vec{f}_j)$. In that case $\vec{f}_l \triangleq R\vec{f}_k$ is also a secondary rotation axis, and $\angle(\vec{v}, \vec{f}_k) = \angle(\vec{v}, \vec{f}_l)$. Obviously, if \vec{f}_k and \vec{f}_l are not adjacent axes, then, there is another secondary rotation axis \vec{f}_i s.t. $\angle(\vec{v}, \vec{f}_i) < \angle(\vec{v}, \vec{f}_k)$, which is a contradiction to the way \vec{f}_k was chosen. If m is odd, then, any angle bisector of two adjacent secondary rotation axes is also a secondary rotation axis.

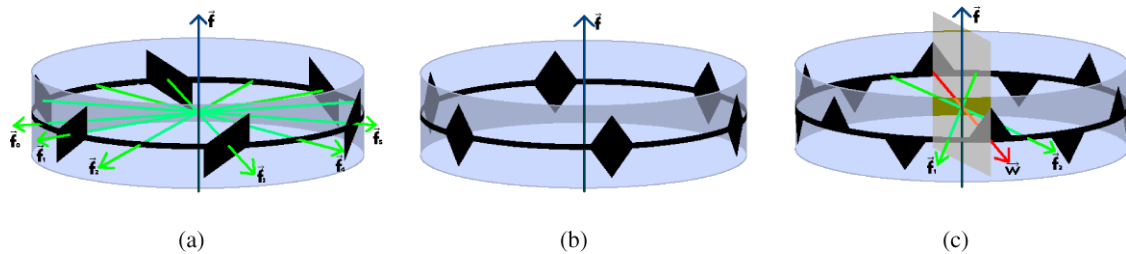
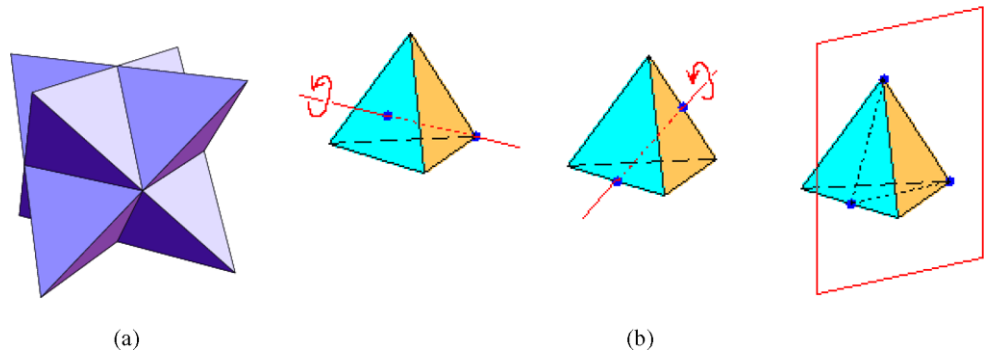


Fig. 4 Dihedral rotations groups. (a) $\mathcal{G}_V = \mathcal{K}_V$ is Dihedric, $m = 6$. \vec{f} is the principal m -fold axis. $\{\vec{f}_j\}_{j=0}^{m-1}$ are the secondary rotation axes. The angle between adjacent secondary rotation axes is $\frac{\pi}{m}$. (b) \mathcal{K}_V is Dihedric, $\mathcal{G}_V \neq \mathcal{K}_V$ and $I \in \mathcal{G}_V$. The rotation axes are the same as those

in (a). (c) \mathcal{K}_V is Dihedric, $\mathcal{G}_V \neq \mathcal{K}_V$ and $I \notin \mathcal{G}_V$. The rotation axes are the same as the rotation axes in (a). Any angle bisector between two adjacent secondary rotation axes spans a reflection plane with the principal axis

Fig. 5 Tetrahedral rotations groups, $\mathcal{G}_V \neq \mathcal{K}_V$. (a) \mathcal{G}_V is Tetrahedric, $I \in \mathcal{G}_V$. (b) \mathcal{G}_V is Tetrahedric, $\mathcal{G}_V \neq \mathcal{K}_V$, $I \notin \mathcal{G}_V$. Left: a threefold rotation axis. Middle: a twofold rotation axis. Right: The reflection plane is spanned by the indicated axes



Assume that \vec{v} is a secondary rotation axis of V , i.e., $\vec{v} = \vec{f}_j$ for some $0 \leq j < m$. If m is even, then, $\vec{f}_k \triangleq O^{\frac{m}{2}} \vec{v}$ is a secondary rotation axis and $\vec{f}_k \perp \vec{v}$. In addition, $\mathcal{B} \triangleq \{\vec{f}, \vec{v}, \vec{f}_k\}$ is an orthogonal basis for \mathbb{R}^3 . Define $\tilde{R} \triangleq RO_k$, where $O_k \in \mathcal{K}_V$ is the secondary rotation associated with \vec{f}_k . By applying \tilde{R} on the elements of \mathcal{B} , it follows that $\tilde{R}\vec{f} = RO_k\vec{f} = -R\vec{f} = -\vec{f}$, $\tilde{R}\vec{v} = RO_k\vec{v} = -R\vec{v} = -\vec{v}$ and $\tilde{R}\vec{f}_k = RO_k\vec{f}_k = R\vec{f}_k = -\vec{f}_k$, i.e. $\tilde{R} = I$, which contradicts to the assumption. \square

Lemma 3.4 Under the conditions of Lemma 3.3, each vector \vec{w} , which bisects the angle between two adjacent secondary rotation axes of V , has a reflection $\tilde{R} \in \mathcal{G}_V$ that satisfies $\tilde{R}\vec{f} = \vec{f}$ and $\tilde{R}\vec{w} = \vec{w}$.

Proof From Lemma 3.3 there is a reflection $R \in \mathcal{G}_V$, which satisfies $R\vec{f} = \vec{f}$ and $R\vec{v} = \vec{v}$, where \vec{v} is an angle bisector between two adjacent secondary rotation axes of V . Let $R_k \triangleq O^k R$, $k = 1, \dots, m-1$, where m is the order of O , which is the principal rotation of V . Then, $R_k \in \mathcal{G}_V$ is a rotation-inversion that satisfies $R_k\vec{f} = \vec{f}$, i.e., R_k has eigenvalue 1, hence, R_k is a reflection. Using the same arguments as in the proof of Lemma 3.3, we get that there is a vector \vec{v}_k , which bisects the angle between two adjacent secondary rotation axes of V that satisfies $R_k\vec{v}_k = \vec{v}_k$. Obviously, $\vec{v}_j = \vec{v}_k$ if and only if $j = k$, i.e., each one of the m angle bisector vectors between two adjacent secondary rotation axes of V has a reflection, which satisfies the lemma. \square

3.2.3 Tetrahedral Rotations Subgroup

Lemma 3.5 (Holden 1971) Let V be a Tetrahedron. If $\mathcal{G}_V \neq \mathcal{K}_V$ and $I \notin \mathcal{G}_V$, then, any twofold axis spans a reflection plane of V with any three-fold axis (see Fig. 5).

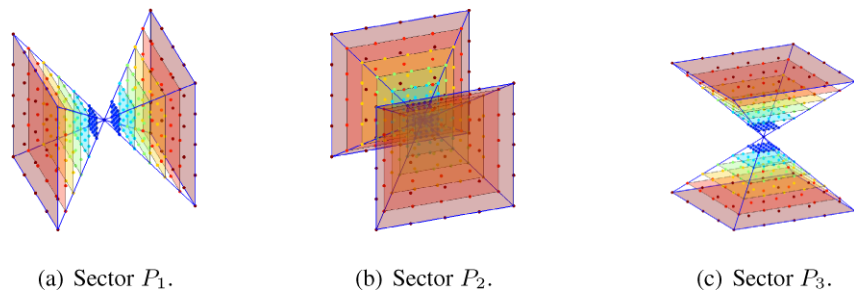
3.3 Properties of the Fourier Transform

The Fourier transform is the main computational tool used by the proposed symmetry detection algorithm. It was shown to be an efficient computational approach in 2D symmetry analysis schemes (Lucchese 2004; Keller and Shkolnisky 2006) that were further discussed in Sect. 2. In this section, we present the Fourier transform properties that are utilized by our 3D symmetry detection algorithm.

For any function $f : \mathbb{R}^3 \rightarrow \mathbb{R}$, whose modulus is square integrable on \mathbb{R}^3 , its 3D Fourier transform, denoted by \hat{f} , is given by $\hat{f}(\vec{w}) \triangleq \iint_{\mathbb{R}^3} f(\vec{x}) e^{-i\langle \vec{w}, \vec{x} \rangle} d\vec{x}$.

Lemma 3.6 Let $f : \mathbb{R}^3 \rightarrow \mathbb{R}$ and let $O \in \mathcal{O}(3)$. Then, $\widehat{\Lambda(O)f} = \Lambda(O)\hat{f}$.

Proof $\widehat{\Lambda(O)f}(\vec{w}) = \iint_{\mathbb{R}^3} \Lambda(O)f(\vec{x}) e^{-i\langle \vec{x}, \vec{w} \rangle} d\vec{x} = \iint_{\mathbb{R}^3} f(O^{-1}\vec{x}) e^{-i\langle \vec{x}, \vec{w} \rangle} d\vec{x}$. Substitute $\vec{z} = O^{-1}\vec{x}$, then, the last integral becomes $\iint_{\mathbb{R}^3} f(\vec{z}) e^{-i\langle O\vec{z}, \vec{w} \rangle} J d\vec{z}$, where J is the Jacobian, i.e. $J = |\frac{\partial \vec{x}}{\partial \vec{z}}| = |\det(O^{-1})|$. Since $O \in \mathcal{O}(3)$, $J = 1$ and $\langle O\vec{z}, \vec{w} \rangle = \langle \vec{z}, O^{-1}\vec{w} \rangle$. It follows that $\widehat{\Lambda(O)f}(\vec{w}) = \iint_{\mathbb{R}^3} f(\vec{z}) e^{i\langle \vec{z}, O^{-1}\vec{w} \rangle} d\vec{z} = \Lambda(O)\hat{f}(\vec{w})$. \square

Fig. 6 The pseudo-polar grid consisting of three sectors

Lemma 3.7 $\mathcal{G}_f = \mathcal{G}_{\hat{f}}$.

Proof Let $O \in \mathcal{G}_f$, then, $\Lambda(O)\hat{f} = \widehat{\Lambda(O)f} = \hat{f}$. The first equality is derived from Lemma 3.6, while the second stems from $O \in \mathcal{G}_f$. If $O \in \mathcal{G}_{\hat{f}}$, then $\widehat{\Lambda(O)f} = \Lambda(O)\hat{f} = \hat{f}$, and by the Fourier transform being bijective we conclude that $\Lambda(O)f = f$, i.e. $O \in \mathcal{G}_f$. \square

It follows from Lemma 3.7 that the Fourier transform of a function retains its symmetrical properties. Hence, instead of analyzing the symmetrical properties of a volume in its spatial representation, we prefer the Fourier domain, where we analyze the volume's translation-invariant representation using the 3D pseudo-polar FFT transform.

3.4 The 3D Pseudo-polar FFT

Given a volume V of size $N \times N \times N$, its 3D discrete Fourier transform, denoted $\hat{V}(\omega_x, \omega_y, \omega_z)$ is given by

$$\hat{V}(\omega_x, \omega_y, \omega_z) \triangleq \sum_{u,v,w=-N/2}^{N/2-1} V(u, v, w) e^{-\frac{2\pi i}{M}(u\omega_x + v\omega_y + w\omega_z)}, \quad (3.3)$$

where $\omega_x, \omega_y, \omega_z \in R$. For ω_x, ω_y and ω_z , which are sampled on the Cartesian grid $(\omega_x, \omega_y, \omega_z) = (m, k, l)$, $m, k, l = -\frac{M}{2}, \dots, \frac{M}{2} - 1$, the discrete Fourier transform in (3.3) becomes

$$\begin{aligned} \hat{V}_{\text{Cart}}(m, k, l) &\triangleq \hat{V}(m, k, l) \\ &= \sum_{u,v,w=-N/2}^{N/2-1} V(u, v, w) e^{-\frac{2\pi i}{M}(um + vk + wl)}, \end{aligned} \quad (3.4)$$

where $m, k, l = -\frac{M}{2}, \dots, \frac{M}{2} - 1$, which is usually referred to as 3D DFT of the volume V .

The 3D pseudo-polar Fourier transform (3DPPFT) (Averbuch and Shkolnisky 2003) evaluates accurately the 3D Fourier transform of a volume on the 3D pseudo-polar grid. Formally, the 3D pseudo-polar grid is given by the set of

samples

$$P \triangleq P_1 \cup P_2 \cup P_3, \quad (3.5)$$

where

$$\begin{aligned} P_1 &\triangleq \left\{ \left(m, -\frac{2k}{N}m, -\frac{2l}{N}m \right) \right\}, \\ P_2 &\triangleq \left\{ \left(-\frac{2k}{N}m, m, -\frac{2l}{N}m \right) \right\}, \\ P_3 &\triangleq \left\{ \left(-\frac{2k}{N}m, -\frac{2l}{N}m, m \right) \right\}, \end{aligned} \quad (3.6)$$

and $k, l = -\frac{N}{2}, \dots, \frac{N}{2}$, $m = -\frac{3N}{2}, \dots, \frac{3N}{2}$, N even. See Fig. 6 for an illustration of the sets P_1, P_2 and P_3 . We define the 3D pseudo-polar Fourier transform of V as the samples of the Fourier transform \hat{V} , given by (3.3), on the 3D pseudo-polar grid P , given by (3.5) and (3.6). Formally, the 3D pseudo-polar Fourier-transform, denoted by \hat{V}_{PP}^s ($s = 1, 2, 3$), is a linear transformation, which defined for $m = -\frac{3N}{2}, \dots, \frac{3N}{2}$ and $k, l = -\frac{N}{2}, \dots, \frac{N}{2}$,

$$\begin{aligned} \hat{V}_{PP}^1(m, k, l) &\triangleq \hat{V}\left(m, -\frac{2k}{N}m, -\frac{2l}{N}m\right) \\ &= \sum_{u,v,w=-N/2}^{N/2-1} V(u, v, w) \\ &\quad \times e^{-\frac{2\pi i}{M}(mu - \frac{2k}{N}mv - \frac{2l}{N}mw)}, \\ \hat{V}_{PP}^2(m, k, l) &\triangleq \hat{V}\left(-\frac{2k}{N}m, m, -\frac{2l}{N}m\right) \\ &= \sum_{u,v,w=-N/2}^{N/2-1} V(u, v, w) \\ &\quad \times e^{-\frac{2\pi i}{M}(-\frac{2k}{N}mu + mv - \frac{2l}{N}mw)}, \\ \hat{V}_{PP}^3(m, k, l) &\triangleq \hat{V}\left(-\frac{2k}{N}m, -\frac{2l}{N}m, m\right) \\ &= \sum_{u,v,w=-N/2}^{N/2-1} V(u, v, w) \\ &\quad \times e^{-\frac{2\pi i}{M}(-\frac{2k}{N}mu - \frac{2l}{N}mv + mw)}, \end{aligned}$$

where \hat{V} is given by (3.3). The set P , given by (3.5), can be written in pseudo-polar coordinates as $P = \{(r_i \cos \theta_j \sin \phi_k, r_i \sin \theta_j \sin \phi_k, r_i \cos \phi_k) \mid (r_i, \theta_j, \phi_k) \in \Gamma\}$, where the set Γ contains all triplets that correspond to points on the pseudo-polar grid P . A full description of the 3DPPFT algorithm is given in Averbuch and Shkolnisky (2003).

3.5 The Angular Difference Function

The Angular Difference Function (ADF) was proposed in Keller et al. (2006) as a computational approach for estimating 3D rotations. Given two 3D volumes, their ADF can be computed with high algebraic accuracy using the 3DPPFT. The ADF can then be used to estimate the relative rotation between two 3D volumes with improved accuracy and robustness to noise.

Let V_1 and V_2 be two volumes, given in pseudo-polar coordinates, i.e., $V_1 = V_1(r_i, \theta_j, \phi_k)$, $V_2 = V_2(r_i, \theta_j, \phi_k)$, $(r_i, \theta_j, \phi_k) \in \Gamma$. The **Angular Difference Function (ADF)** of V_1 and V_2 on the interval $[0, r_0]$ is

$$\Delta_{V_1, V_2}(\theta_j, \phi_k) \triangleq \sum_{0 \leq r_i \leq r_0} |V_1(r_i, \theta_j, \phi_k) - V_2(r_i, \theta_j, \phi_k)|.$$

It follows that $\Delta_{V_1, V_2}(\theta_j, \phi_k) \geq 0$, and equality is obtained if and only if $V_1(\cdot, \theta_j, \phi_k) = V_2(\cdot, \theta_j, \phi_k)$. Whenever the notation $\Delta_{V_1, V_2}(\vec{f})$ is used, it represents $\Delta_{V_1, V_2}(\theta_j, \phi_k)$, where θ_j and ϕ_k are the pseudo-polar angular coordinates of \vec{f} .

4 The 3D Symmetry Detection Algorithm

In this section, we introduce the 3D Symmetry Detection Algorithm (3DSDA). We first find \mathcal{K}_V , the group of rotational symmetries of V . Then, in order to infer the full symmetry group \mathcal{G}_V , we detect a single rotation-inversion. The algorithm is based on the analysis of the ADF of the given volume V with respect to rotated and rotated-inverted replicas of V . Since the center of mass of a given volume is unique, it is invariant under any symmetry of the volume. Hence, all the rotations and rotation-inversions transforms have to be applied such that the center of mass is fixed. The center of mass of V is defined by $\frac{\sum_{x \in C} V(x)x}{\sum_{x \in C} V(x)}$, where $C \subset \mathbb{R}^3$ is the support of V .

4.1 Detecting a Single Rotation Axis

We start by detecting a single rotation axis (and its order) of the input volume V . Our approach is based on the ADF of V and its arbitrary rotated replica, $\tilde{V} \triangleq \Lambda(\tilde{O})V$, where \tilde{f}_0 is the rotation axis and δ the rotation angle of \tilde{O} .

Let \vec{f} be the rotation axis of $\tilde{O}O$, i.e., $\tilde{O}O\vec{f} = \vec{f}$. From (3.2) we have that $\tilde{V}(\vec{f}) = \Lambda(\tilde{O})V(\vec{f}) = \Lambda(\tilde{O})\Lambda(O)V(\vec{f}) = \Lambda(\tilde{O}O)V(\vec{f}) = V((\tilde{O}O)^{-1}\vec{f}) = V(\vec{f})$,

hence, $\Delta_{V, \tilde{V}}(\vec{f}) = 0$. It follows that the zeros of $\Delta_{V, \tilde{V}}$ are the eigenvectors of $\tilde{O}O$.

Remark 4.1 If for any $O \in \mathcal{K}_V$, the rotation axis of $\tilde{O}O$ is not one of the rotation axes of V , then, any rotation of the form $\tilde{O}O$, $O \in \mathcal{K}_V$, has a different rotation axis.

Proof Let $O_1, O_2 \in \mathcal{K}_V$ and assume that \vec{f} is a common rotation axis of $\tilde{O}O_1$ and $\tilde{O}O_2$, i.e., $\tilde{O}O_1\vec{f} = \vec{f}$ and $\tilde{O}O_2\vec{f} = \vec{f}$, then, $O_1^{-1}O_2\vec{f} = \vec{f}$, i.e., \vec{f} is a rotation axis of V , which contradicts the assumption. \square

As the number of symmetry axes of V is finite, the probability that Remark 4.1 is violated tends to zero. Let \vec{f} be an n -fold axis of V and let O be the rotation of order $n > 1$ associated with \vec{f} , i.e.,

$$O\vec{f} = \vec{f}. \quad (4.1)$$

The rotation angle is $\gamma = \frac{2\pi}{n}$. For $k = 1, 2, \dots, n-1$ we define the linear transformations

$$T_k \triangleq O^k - E. \quad (4.2)$$

Obviously, $\text{null}(T_k) = \text{span}\{\vec{f}\}$. In addition, T_k is a normal operator, whose null-space and image are orthogonal

$$\text{Im}(T_k) = \text{span}\{\vec{f}\}^\perp. \quad (4.3)$$

We denote by \vec{f}_k the rotation axis of $\tilde{O}O^k$, $k = 0, 1, \dots, n-1$, i.e.,

$$\tilde{O}O^k\vec{f}_k = \vec{f}_k. \quad (4.4)$$

From (4.2) and (4.4), we get $\langle \vec{f}_0, T_k\vec{f}_k \rangle = \langle \vec{f}_0, (O^k - E)\vec{f}_k \rangle = \langle \tilde{O}\vec{f}_0, \tilde{O}(O^k - E)\vec{f}_k \rangle = \langle \vec{f}_0, \tilde{O}O^k\vec{f}_k - \tilde{O}\vec{f}_k \rangle = \langle \vec{f}_0, \vec{f}_k - \tilde{O}\vec{f}_k \rangle = \langle \vec{f}_0, (E - \tilde{O})\vec{f}_k \rangle = \langle (E - \tilde{O})^* \vec{f}_0, \vec{f}_k \rangle = \langle (E - \tilde{O}^{-1})\vec{f}_0, \vec{f}_k \rangle = \langle \vec{f}_0 - \tilde{O}^{-1}\vec{f}_0, \vec{f}_k \rangle = \langle \vec{0}, \vec{f}_k \rangle = 0$, i.e., $\vec{f}_0 \perp T_k\vec{f}_k$. \square

By combining (4.3) and (4.5) it follows that $T_k\vec{f}_k \in \text{span}\{\vec{f}, \vec{f}_0\}^\perp$, $k = 1, 2, \dots, n-1$. Under the assumption of Remark 4.1, \vec{f} and \vec{f}_0 are linearly independent and $T_k\vec{f}_k \neq \vec{0}$, $k = 1, 2, \dots, n-1$. Hence, we conclude that $\dim\{\text{span}\{T_k\vec{f}_k\}_{k=1}^{n-1}\} = 1$ and the next corollary holds:

Corollary 4.1 *There exist a non-zero vector $\vec{\omega}$ and a scalar a_k s.t. $T_k\vec{f}_k = a_k\vec{\omega}$, $k = 1, 2, \dots, n-1$.*

Lemma 4.1 *Under the assumption of Remark 4.1, each pair of vectors from $\{\vec{f}_j\}_{j=0}^{n-1}$ is linearly independent.*

Proof Assume that $\vec{f}_j = a\vec{f}_k$, $a \in \mathbb{R}$, $j < k$, then, by (4.4) we get that $\tilde{O}O^j\vec{f}_j = a\tilde{O}O^k\vec{f}_k$. It follows that $\vec{f}_j = aO^{k-j}\vec{f}_k = O^{k-j}\vec{f}_j$, i.e., \vec{f}_j is the rotation axis of O , which contradicts the assumption of Remark 4.1. \square

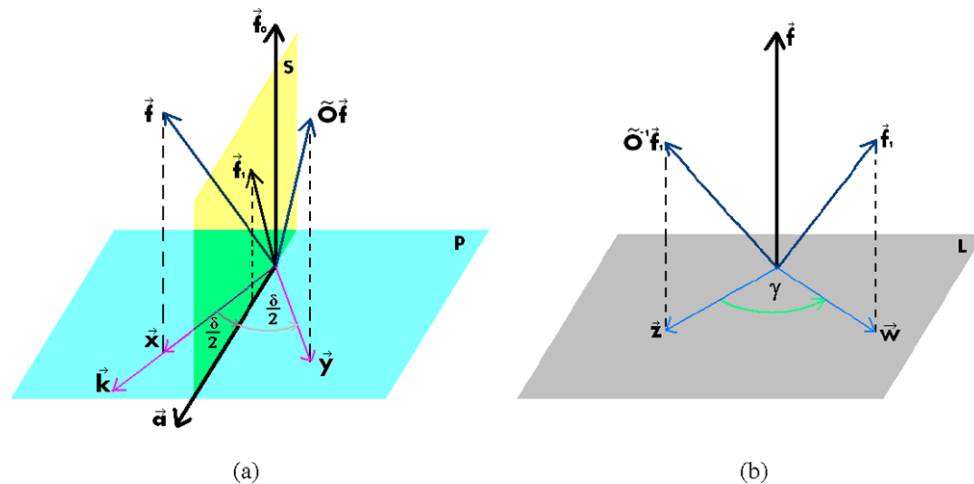


Fig. 7 The geometric relations between \vec{f} and \mathcal{S} . (a) \vec{f}_0 and δ are the rotation axis and the rotation angle of \tilde{O} , respectively. \vec{f}_0 and \vec{f}_1 belong to \mathcal{S} , which is the CP of O in respect to \tilde{O} . \mathcal{P} is the perpendicular plane to \vec{f}_0 . \vec{x} and \vec{y} are the orthogonal projections of \vec{f} and

$\tilde{O}\vec{f}$ on \mathcal{P} , respectively. \vec{a} is the normalized orthogonal projection of \vec{f}_1 on \mathcal{P} . $\vec{k} = \tilde{O}^{-\frac{1}{2}}\vec{a}$. (b) \vec{f} and γ are the rotation axis and the rotation angle of O , respectively. \mathcal{L} is the perpendicular plane to \vec{f} . \vec{w} and \vec{z} are the orthogonal projections of \vec{f}_1 and $\tilde{O}^{-1}\vec{f}_1$, respectively

Theorem 4.1 $\vec{f}_j \in \text{span}\{\vec{f}_0, \vec{f}_1\}$, $j = 2, \dots, n-1$.

Proof According to Corollary 4.1 and (4.2), there is a scalar $b \neq 0$ s.t. $\tilde{O}T_j\vec{f}_j = \tilde{O}bT_1\vec{f}_1 = b[\tilde{O}O\vec{f}_1 - \tilde{O}\vec{f}_1] = b\vec{f}_1 - b\tilde{O}\vec{f}_1$. Moreover, we have that $\tilde{O}T_j\vec{f}_j = \tilde{O}O^j\vec{f}_j - \tilde{O}\vec{f}_j = \vec{f}_j - \tilde{O}\vec{f}_j$. Thus, it follows that $\tilde{O}(b\vec{f}_1 - \vec{f}_j) = b\vec{f}_1 - \vec{f}_j$, i.e., $b\vec{f}_1 - \vec{f}_j$ is either $\vec{0}$ or proportional to \vec{f}_0 . According to Lemma 4.1, the first option is invalid, i.e., $b\vec{f}_1 - \vec{f}_j = c\vec{f}_0$, or, in other words, $\vec{f}_j \in \text{span}\{\vec{f}_0, \vec{f}_1\}$, $j = 2, \dots, n-1$. \square

In practice, Theorem 4.1 states that the rotation axes of $\tilde{O}O^k$, $k = 0, 1, \dots, n-1$, belong to a single plane in \mathbb{R}^3 , i.e., to $\text{span}\{\vec{f}_0, \vec{f}_1\}$. We call this plane the **Characteristic Plane (CP) of O with respect to \tilde{O}** . Next, we reveal the geometric relations between \vec{f} , which is the rotation axis of O , and the CP of O , which is denoted by \mathcal{S} (see Fig. 7). By applying the Gram-Schmidt procedure, we compute an orthonormal basis for \mathcal{S} . Assume that \vec{f}_0 is normal, i.e., $\|\vec{f}_0\| = 1$. Let

$$\vec{b} \triangleq \vec{f}_1 - \langle \vec{f}_1, \vec{f}_0 \rangle \vec{f}_0 \quad \text{and} \quad \vec{a} \triangleq \vec{b} / \|\vec{b}\|.$$

Then, $\{\vec{f}_0, \vec{a}\}$ is an orthonormal basis for \mathcal{S} . Denote

$$\vec{x} \triangleq \vec{f} - \langle \vec{f}, \vec{f}_0 \rangle \vec{f}_0 \quad \text{and} \quad \vec{y} \triangleq \tilde{O}\vec{f} - \langle \tilde{O}\vec{f}, \vec{f}_0 \rangle \vec{f}_0 \quad (4.6)$$

as the orthogonal projections of \vec{f} and $\tilde{O}\vec{f}$, respectively, on the plane orthogonal to \vec{f}_0 , denoted by \mathcal{P} , then \vec{x} , \vec{y} and \vec{a} belong to \mathcal{P} , and the following equations hold:

$$\langle \vec{f}, \vec{f}_0 \rangle = \langle \tilde{O}\vec{f}, \vec{f}_0 \rangle, \quad (4.7)$$

$$\langle \vec{f}, \vec{f}_1 \rangle = \langle \tilde{O}\vec{f}, \vec{f}_1 \rangle \quad (4.8)$$

and

$$\angle(\vec{a}, \vec{x}) = \angle(\vec{a}, \vec{y}). \quad (4.9)$$

From (4.4) we get

$$\tilde{O}\vec{x} = \tilde{O}\vec{f} - \langle \vec{f}, \vec{f}_0 \rangle \tilde{O}\vec{f}_0 = \tilde{O}\vec{f} - \langle \tilde{O}\vec{f}, \vec{f}_0 \rangle \vec{f}_0 = \vec{y}, \quad (4.10)$$

and following (4.4) and (4.10) we conclude that

$$\tilde{O}^{-\frac{1}{2}}\vec{a} = \vec{x} / \|\vec{x}\|, \quad (4.11)$$

where $\tilde{O}^{-\frac{1}{2}}$ denotes the rotation by angle $-\frac{\delta}{2}$ around \vec{f}_0 . Let $\vec{k} \triangleq \tilde{O}^{-\frac{1}{2}}\vec{a}$, then by (4.6) and (4.11) we derive Corollary 4.2.

Corollary 4.2 $\vec{f} \in \text{span}\{\vec{k}, \vec{f}_0\}$, i.e. $\vec{f} = b\vec{f}_0 + c\vec{k}$ (see Fig. 7(a)).

At this point, γ , which is the rotation angle of O , is already known since $\gamma = \frac{2\pi}{n}$, where n is the number of detected vectors, i.e., the vectors that satisfy $\Delta_{V, \vec{v}}(\vec{f}) = 0$. Our next goal is to recover b and c , s.t. Corollary 4.2 holds.

Let $\vec{w} \triangleq \vec{f}_1 - \langle \vec{f}_1, \vec{f} \rangle \vec{f}$ and $\vec{z} \triangleq \tilde{O}^{-1}\vec{f}_1 - \langle \tilde{O}^{-1}\vec{f}_1, \vec{f} \rangle \vec{f}$ be the orthogonal projections of \vec{f}_1 and $\tilde{O}^{-1}\vec{f}_1$, respectively, on the plane that is perpendicular to \vec{f} , denoted by \mathcal{L} (see Fig. 7(b)).

Lemma 4.2 $\angle(\vec{w}, \vec{z}) = \gamma$.

Proof Since \vec{w} and \vec{z} both belong to the plane that is perpendicular to \vec{f} , it suffices to prove that

$$O\vec{w} = \vec{z}. \quad (4.12)$$

From (4.1), (4.4), (4.7) and (4.8), we get $O\vec{\omega} = O\vec{f}_1 - \langle \vec{f}_1, \vec{f}_0 \rangle O\vec{f} = \vec{O}^{-1}\vec{f}_1 - \langle \vec{f}_1, \vec{f} \rangle \vec{f} = \vec{O}^{-1}\vec{f}_1 - \langle \vec{O}^{-1}\vec{f}_1, \vec{f} \rangle \vec{f} = \vec{z}$. \square

This is illustrated in Fig. 7(b).

Lemma 4.3 $\langle \vec{f}_1, \vec{k} \rangle = \langle \vec{f}_1, \vec{O}\vec{k} \rangle$.

According to Lemma 4.2, it remains to recover b and c s.t.

$$\frac{\langle \vec{w}, \vec{z} \rangle}{\|\vec{w}\| \|\vec{z}\|} = \cos(\gamma) \quad (4.13)$$

holds. We reformulate (4.13) to explicitly reference b and c . From (4.4), the normalization of \vec{f} , Corollary 4.2 and Lemma 4.3, it follows that $\langle \vec{w}, \vec{z} \rangle = \langle \vec{O}\vec{f}_1, \vec{f}_1 \rangle - (b\langle \vec{f}_1, \vec{f}_0 \rangle + c\langle \vec{f}_1, \vec{k} \rangle)^2$. In addition, if \vec{f}_1 is normal, we get $\|\vec{w}\|^2 = 1 - [b\langle \vec{f}_1, \vec{f}_0 \rangle + c\langle \vec{f}_1, \vec{k} \rangle]^2$. From (4.12) we get $\|\vec{w}\| = \|\vec{z}\|$. Hence, by substituting $g = \langle \vec{O}\vec{f}_1, \vec{f}_1 \rangle$, $h = \langle \vec{f}_1, \vec{f}_0 \rangle$ and $j = \langle \vec{f}_1, \vec{k} \rangle$, (4.13) becomes

$$\frac{g - (bh + cj)^2}{1 - (bh + cj)^2} = \cos(\gamma). \quad (4.14)$$

An additional equation is obtained from the normalization of \vec{f} , i.e.,

$$b^2 + c^2 = 1. \quad (4.15)$$

The solution of (4.14) and (4.15) is $c_{1,2} = \frac{\pm Gj + h\sqrt{h^2 + j^2 - G^2}}{j^2 + h^2}$, where $G = \sqrt{\frac{g - \cos(\gamma)}{1 - \cos(\gamma)}}$. $b_{1,2}$ can be found with respect to $c_{1,2}$. Only a single pair of solutions (b_j, c_j) , $j = 1, 2$, satisfies (4.14).

Algorithm 1 detects a single rotation in the symmetry group of a volume V given $\Delta_{V,\vec{v}}$.

Algorithm 1 Detecting a single rotation axis

Input: The set $\mathcal{A} \triangleq \{\vec{f} \in \mathbb{R}^3 : \Delta_{V,\vec{v}}(\vec{f}) = 0\}$, which belongs to a single CP, where $\vec{V} = \Lambda(\vec{O})V$ and the rotation axis \vec{f}_0 and angle δ of \vec{O} .

Output: A single rotation $O \in \mathcal{K}_V$

- 1: Define $n \triangleq |\mathcal{A}|$.
- 2: If $n = 1$, i.e. $\mathcal{A} = \{\vec{f}_0\}$, stop—then the output is $O = E$.
- 3: Choose $\vec{f}_1 \in \mathcal{A}$, $\vec{f}_1 \neq \vec{f}_0$. Compute $\vec{k} \triangleq \vec{O}^{-\frac{1}{2}} \left(\frac{\vec{f}_1 - \langle \vec{f}_1, \vec{f}_0 \rangle \vec{f}_0}{\|\vec{f}_1 - \langle \vec{f}_1, \vec{f}_0 \rangle \vec{f}_0\|} \right)$, where $\vec{O}^{-\frac{1}{2}}$ is the rotation whose rotation axis and rotation angle are \vec{f}_0 and $-\frac{\delta}{2}$, respectively (see (3.1)).
- 4: Solve (4.14) and (4.15) for b and c .
- 5: Compute the rotation matrix O , whose rotation axis and angle are $\vec{f} \triangleq b\vec{f}_0 + c\vec{k}$ and $\gamma \triangleq \frac{2\pi}{n}$, respectively (see (3.1)).

4.2 Recovering All of the Rotations Axes

If all the CPs of a given volume are distinct, then Algorithm 1 can be applied to each of the CPs separately. Each of the CPs contains \vec{f}_0 . The recovery of the CPs is straightforward. The following lemma provides the required conditions for having distinct CPs.

Lemma 4.4 Let \vec{v}_1 and \vec{v}_2 be two rotation axes of V , which are associated with CPs \mathcal{S}_1 and \mathcal{S}_2 . If \vec{f}_0 does not belong to $\text{span}\{\vec{v}_1, \vec{v}_2\}$, then $\mathcal{S}_1 \neq \mathcal{S}_2$.

Proof Assume that $\mathcal{S}_1 = \mathcal{S}_2$. Since $\mathcal{S}_1 = \text{span}\{\vec{f}_0, \vec{v}_1\}$ and $\mathcal{S}_2 = \text{span}\{\vec{f}_0, \vec{v}_2\}$, it follows that \vec{v}_1, \vec{v}_2 and \vec{f}_0 are linearly dependent. Since \vec{v}_1 and \vec{v}_2 are linearly independent, it follows that $\vec{f}_0 \in \text{span}\{\vec{v}_1, \vec{v}_2\}$, which contradicts the assumption. \square

We assume that \vec{O} , which is arbitrarily chosen, satisfies the assumptions of Remark 4.1 and Lemma 4.4. Recall that each CP contains \vec{f}_0 and any detected vector \vec{g} can be classified to its corresponding CP by computing $\vec{g} \times \vec{f}_0$. Algorithm 2 presents the computation of the different CPs given the ADF $\Delta_{V,\vec{v}}$.

The complexity of Algorithm 2 is $O(m)$, where $m = |D|$. Due to (3.5), $m = O(N^2)$.

4.3 Detecting a Single Rotation-inversion

In this section, we describe four algorithms that detect a single rotation-inversion of a volume V , whose rotations subgroup \mathcal{K}_V is already known. Each algorithm relates to a different type of rotations subgroup: Trivial, Cyclic, Dihedral and Tetrahedral. The two additional types of rotations subgroups (Octahedral and Icosahedral) are associated with the inversion, as mentioned in Sect. 3.2. This completes the entire process of symmetry group detection. Recall that if $\mathcal{G}_V \neq \mathcal{K}_V$ and $I \notin \mathcal{G}_V$, then, \mathcal{K}_V is either the trivial group $\{E\}$ or Cyclic or Dihedral or Tetrahedral. If \mathcal{K}_V is Dihedral or Tetrahedral, then, from Lemmas 3.4 and 3.5, the geometric relation between the reflection planes and the rotation axes are well known. Hence, it remains to establish a method for detecting a single reflection $R \in \mathcal{G}_V$, where \mathcal{K}_V is either trivial or Cyclic.

Algorithm 2 Detection of all the CPs

Input: $\Delta_{V,\vec{v}}$.

Output: Partition of the detected vectors to disjoint CPs, $\mathcal{S}_1, \mathcal{S}_2, \dots, \mathcal{S}_k$.

- 1: Define $D = \{\vec{f} : \Delta_{V,\vec{v}}(\vec{f}) = 0\}$.
- 2: Divide D to disjoint subgroups $\mathcal{S}_1, \mathcal{S}_2, \dots, \mathcal{S}_k$, such that two vectors $\vec{f}, \vec{g} \in D$ belong to the same subgroup if $\vec{f} \times \vec{f}_0$ and $\vec{g} \times \vec{f}_0$ are linearly dependent.

Let

$$\tilde{V} \triangleq \Lambda(\tilde{R})V, \quad (4.16)$$

where \tilde{R} is an arbitrary rotation-inversion. Suppose that $S \in \mathcal{G}_V$ is a rotation-inversion, and that \vec{f} is the rotation axis of $\tilde{R}S$. Then, $(\tilde{R}S)^{-1}\vec{f} = \vec{f}$. In addition, from (3.2) and (4.16), we get

$$\begin{aligned} \tilde{V}(\vec{f}) &= \Lambda(\tilde{R})V(\vec{f}) = \Lambda(\tilde{R})\Lambda(S)V(\vec{f}) = \Lambda(\tilde{R}S)V(\vec{f}) \\ &= V((\tilde{R}S)^{-1}\vec{f}) = V(\vec{f}), \end{aligned}$$

hence, $\Delta_{V,\tilde{V}}(\vec{f}) = 0$. It follows that the zeros of $\Delta_{V,\tilde{V}}(\vec{f}) = 0$ are the eigenvectors of $\tilde{R}S$.

Remark 4.2 For any rotation-inversion $S \in \mathcal{G}_V$, if the rotation axis of $\tilde{R}S$ is not one of the rotation axes of V , then, any rotation of the form $\tilde{R}S$, $S \in \mathcal{G}_V$ has a unique rotation axis.

Proof Let $S_1, S_2 \in \mathcal{G}_V$ be two rotation-inversions. Assume that \vec{f} is a common rotation axis of $\tilde{R}S_1$ and $\tilde{R}S_2$, i.e., $\tilde{R}S_1\vec{f} = \vec{f}$ and $\tilde{R}S_2\vec{f} = \vec{f}$, then, $S_1^{-1}S_2\vec{f} = \vec{f}$, i.e., \vec{f} is a rotation axis of V . \square

Under the assumption of Remark 4.2, it follows that all the eigenvectors of $\tilde{R}S$ can be detected from $\Delta_{V,\tilde{V}}$ and they are all different. Next, we describe our approach for detecting a single rotation-inversion in \mathcal{G}_V given \mathcal{K}_V of different classes:

4.3.1 \mathcal{K}_V is trivial

Assume that $\mathcal{K}_V = \{E\}$. If $\mathcal{G}_V \neq \mathcal{K}_V$ and $I \notin \mathcal{G}_V$, then we get $\mathcal{G}_V = \{E, R\}$, where R is a reflection. Let \tilde{R} be a rotation-inversion and let $\tilde{V} \triangleq \Lambda(\tilde{R})V$. Then, the vector \vec{f} , which satisfies $\Delta_{V,\tilde{V}}(\vec{f}) = 0$, is the rotation axis of $\tilde{R}R$, i.e.,

$$R\vec{f} = \tilde{R}^{-1}\vec{f}. \quad (4.17)$$

Equation (4.17) has a unique solution with respect to R , and thus we formulate Algorithm 3 whose computational complexity is of $O(N^2)$.

Algorithm 3 Detection of a single reflection, where $\mathcal{K}_V = \{E\}$

Input: $\Delta_{V,\tilde{V}}$, where $\tilde{V} = \Lambda(\tilde{R})V$ and \tilde{R} is an arbitrary rotation-inversion, where $\mathcal{K}_V = \{E\}$ and $I \notin \mathcal{G}_V$.

Output: A single rotation-inversion $R \in \mathcal{G}_V$.

- 1: If there is no vector \vec{f} , s.t. $\Delta_{V,\tilde{V}}(\vec{f})$, return null.
- 2: If $\Delta_{V,\tilde{V}}(\vec{f}) = 0$, return R , which is the solution of $R\vec{f} = \tilde{R}^{-1}\vec{f}$.

4.3.2 \mathcal{K}_V is Cyclic

Let $\mathcal{K}_V = \langle O \rangle$ is a cyclic group of order n , $\mathcal{G}_V \neq \mathcal{K}_V$ and $I \notin \mathcal{G}_V$. Suppose that the reflection $R_{\vec{f}} \notin \mathcal{G}_V$, where \vec{f} is the rotation axis of O . Let \vec{w} be a vector, which satisfies $\Delta_{V,\tilde{V}}(\vec{w}) = 0$. Then, according to Lemma 3.1, there is a reflection $S \in \mathcal{G}_V$ s.t.

$$S\vec{w} = \tilde{R}^{-1}\vec{w}. \quad (4.18)$$

Equation (4.18) has a unique solution for S and we formulate Algorithm 4 whose complexity is $O(N^3)$, due to its first step.

4.3.3 \mathcal{K}_V is Dihedric

Following Lemma 3.4, we formulate Algorithm 5, whose computational complexity is $O(N^3)$, due to its last step.

4.3.4 \mathcal{K}_V is Tetrahedric

Following Lemma 3.5, we derive Algorithm 6, whose computational complexity is $O(N^3)$, due to its last step.

4.4 The Complete 3DSDA

Algorithm 7 summarizes our proposed symmetry detection and analysis scheme that utilizes Algorithms 1–6. Its computational complexity is of $O(N^3 \log(N))$, due to steps 2 and 10.

Algorithm 4 Detection of a single reflection, where \mathcal{K}_V is Cyclic.

Input: A Cartesian representation of V , $\Delta_{V,\tilde{V}}$, where $\tilde{V} = \Lambda(\tilde{R})V$ and \tilde{R} is an arbitrary rotation-inversion, where \mathcal{K}_V is Cyclic, \vec{f} is V 's rotation axis and $I \notin \mathcal{G}_V$.

Output: A single rotation-inversion $S \in \mathcal{G}_V$.

- 1: If $V = \Lambda(R_{\vec{f}})V$ return $S = R_{\vec{f}}$.
- 2: If there is no vector \vec{w} , s.t. $\Delta_{V,\tilde{V}}(\vec{w})$, return null.
- 3: If $\Delta_{V,\tilde{V}}(\vec{w})$, S is the solution of $S\vec{w} = \tilde{R}^{-1}\vec{w}$.

Algorithm 5 Detection of a single reflection, where \mathcal{K}_V is Dihedric.

Input: An $N \times N \times N$ Dihedron V given by its Cartesian representation, its principal rotation axis \vec{f} and two of its secondary adjacent axes \vec{f}_1 and \vec{f}_2 .

Output: A single rotation-inversion $R \in \mathcal{G}_V$.

- 1: Compute the reflection R , whose reflection plane is spanned by \vec{f} and \vec{w} , where \vec{w} is the angle bisector between \vec{f}_1 and \vec{f}_2 .
- 2: If $V = \Lambda(R)V$, return R . Otherwise, return null.

Algorithm 6 Detection of a single reflection, where \mathcal{K}_V is Tetrahedric.

Input: An $N \times N \times N$ Tetrahedron V given by its Cartesian representation, one of its twofold axes \vec{f} and one of its threefold axes \vec{g} .

Output: A single rotation-inversion $R \in \mathcal{G}_V$.

- 1: Compute the reflection R , whose reflection plane is spanned by \vec{f} and \vec{g} .
- 2: If $V = \Lambda(R)V$, return R . Otherwise, return null.

Algorithm 7 3D Symmetry Detection

Input: An $N \times N \times N$ volume B given in a Cartesian representation.

Output: \mathcal{G}_B .

- 1: $\tilde{B} \triangleq \Lambda(\tilde{O})B$, where \tilde{O} is an arbitrary rotation whose axis is \vec{f}_0 and its rotation angle is δ (see (3.1) and (3.2)).
- 2: $V \triangleq \mathcal{F}_{PP}(B)$ and $\tilde{V} \triangleq \mathcal{F}_{PP}(\tilde{B})$, where \mathcal{F}_{PP} is the 3DPPFT.
- 3: Compute $\Delta_{V,\tilde{V}}$.
- 4: Apply Algorithm 2 to $\Delta_{V,\tilde{V}}$. Let $\mathcal{S}_1, \mathcal{S}_2, \dots, \mathcal{S}_k$ be its output.
- 5: Compute \mathcal{K}_B by applying Algorithm 1 to $\mathcal{S}_i, i = 1, 2, \dots, k, \vec{f}_0$ and δ .
- 6: If $B = \Delta(I)B$ stop. Then, $\mathcal{G}_B = \mathcal{K}_B \cup I\mathcal{K}_B$.
- 7: If \mathcal{K}_B is Dihedric, apply Algorithm 5 to B and to two of its secondary adjacent axes \vec{f}_1 and \vec{f}_2 . Let R be its output. Return $\mathcal{G}_B = \mathcal{K}_B \cup R\mathcal{K}_B$.
- 8: If \mathcal{K}_B is Tetrahedric, apply Algorithm 6 to B , to one of its twofold axes \vec{f} and to one of its threefold axes \vec{g} . Let R be its output. Return $\mathcal{G}_B = \mathcal{K}_B \cup R\mathcal{K}_B$.
- 9: $\tilde{B} \triangleq \Lambda(\tilde{R})B$, where \tilde{R} is an arbitrary rotation-inversion (see (3.2)).
- 10: $V \triangleq \mathcal{F}_{PP}(B)$ and $\tilde{V} \triangleq \mathcal{F}_{PP}(\tilde{B})$, where \mathcal{F}_{PP} is the 3DPPFT.
- 11: Compute $\Delta_{V,\tilde{V}}$.
- 12: If \mathcal{K}_B is trivial, apply Algorithm 3 to $\Delta_{V,\tilde{V}}$. Let R be its output. Return $\mathcal{G}_B = \mathcal{K}_B \cup R\mathcal{K}_B$.
- 13: If \mathcal{K}_B is Cyclic, apply Algorithm 4 to $\Delta_{V,\tilde{V}}$ where V 's rotation axis is \vec{f}_0 . Let R be its output. Return $\mathcal{G}_B = \mathcal{K}_B \cup R\mathcal{K}_B$.

5 Experimental Results

In this section, we experimentally verify the proposed symmetry detection and analysis scheme by applying it to different types of volumes. The first three are synthetic volumes whose rotations subgroups are cyclic, trivial and Dihedric, respectively. For sake of clarity, we detail the different steps in applying the proposed 3DSDA scheme to the first volume, while depicting the intermediate and final results of the algorithm. The other three volumes are real MRI scans

that demonstrate the applicability of our scheme to analyzing real volumes with imperfect symmetry and with an additive noise. The tested volumes are all of size $64 \times 64 \times 64$. Our results exemplify that despite of the low resolution and noisy volumes, the 3DSDA is robust and accurate. The results are summarized in Tables 1–6.

We start by applying the proposed scheme to the square pyramid depicted in Fig. 8a. We follow each step of its symmetry analysis to illustrate the applicability of our scheme.

5.1 Step-by-Step Evolution of the Application of the 3DSDA to the Example in Fig. 8(a)

Let B be the square pyramid depicted in Fig. 8(a). The associated symmetries group consists of a single cyclic subgroup of rotations and four reflections.

Step 7-1

$\tilde{B} \triangleq \Lambda(\tilde{O})B$ is the rotated replica of B , shown in Fig. 8(b). The rotation axis of \tilde{O} is $\vec{f}_0 = (-0.8370, -0.5172, 0.1787)^t$ and the rotation angle of O is $\delta = 262^\circ$.

Step 7-2

$V \triangleq \mathcal{F}_{PP}(B)$, $\tilde{V} \triangleq \mathcal{F}_{PP}(\tilde{B})$.

Step 7-3

$\Delta_{V,\tilde{V}}$ is the ADF of V and \tilde{V} —see Fig. 8(c).

Step 7-4

There are four detected vectors which are all related to a single CP—see Fig. 8(d). It follows that \mathcal{K}_V is Cyclic of order four.

Step 7-5

$$O = \begin{pmatrix} 0.0003 & -0.9998 & 0.0205 \\ 0.9999 & 0 & -0.0135 \\ 0.0135 & 0.0205 & 0.9997 \end{pmatrix}.$$

Thus, we conclude that $\mathcal{K}_V = \{E, O, O^2, O^3\}$.

Step 7-6

Since $B \neq \Lambda(I)B$, $I \notin \mathcal{G}_V$ (see Fig. 8(e)).

Step 7-9

$\tilde{B}_1 \triangleq \Lambda(\tilde{R})B$ where \tilde{R} is an arbitrary rotation-inversion—see Fig. 8(f).

Step 7-10 and 11

Δ_{V,\tilde{V}_1} is the ADF of V and \tilde{V}_1 —see Fig. 8(h).

Step 4-1

$V \neq \Lambda(R_{\vec{f}})V$ —see Fig. 8(g).

Step 4-3

$$S = \begin{pmatrix} -0.9994 & 0.0315 & 0.0126 \\ 0.0315 & 0.9995 & -0.0002 \\ 0.0126 & -0.0002 & 0.9999 \end{pmatrix}.$$

It follows that $\mathcal{G}_V = \{E, O, O^2, O^3, S, SO, SO^2, SO^3\}$ (see Table 1).

Tables 1–6 summarize the result after the application of our scheme to different volumes. For all volumes, Column (a) shows the known symmetries of the volume B ,

Fig. 8 Detecting the Symmetries of a pyramid.
(a) The pyramid B .
(b) A rotated replica of B , $\tilde{B} \triangleq \Lambda(\tilde{O})B$. **(c)** Pseudo-polar representation of the ADF $\Delta_{B,\tilde{B}}$. **(d)** The CP which the detected vectors span. **(e)** The inverted pyramid $\tilde{B} \triangleq \Lambda(I)B$.
(f) A rotated-inverted replica of B , $\tilde{B}_1 \triangleq \Lambda(\tilde{R})B$. **(g)** Δ_{B,\tilde{B}_1} . \vec{w}_0 is the point of view for Δ_{B,\tilde{B}_1}

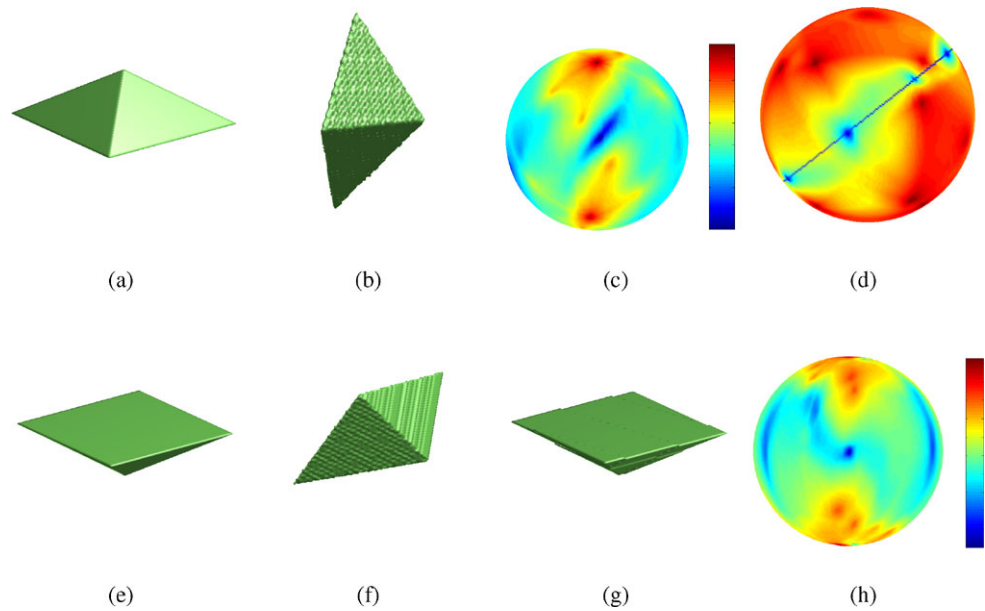


Table 1 Detected symmetries of a pyramid








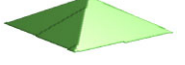
(a) Known symmetry K	(b) Detected symmetry D	(c) $\ K - D\ $	(d) $ \epsilon $	(e) $\Lambda(D)B$
$E = \begin{pmatrix} 1 & 0 & 0 \\ 0 & 1 & 0 \\ 0 & 0 & 1 \end{pmatrix}$	$E = \begin{pmatrix} 1 & 0 & 0 \\ 0 & 1 & 0 \\ 0 & 0 & 1 \end{pmatrix}$	0	0	
$o = \begin{pmatrix} 0 & -1 & 0 \\ 1 & 0 & 0 \\ 0 & 0 & 1 \end{pmatrix}$	$O = \begin{pmatrix} 0.0003 & -0.9998 & 0.0205 \\ 0.9999 & 0 & -0.0135 \\ 0.0135 & 0.0205 & 0.9997 \end{pmatrix}$	0.0245	0.9946°	
$o^2 = \begin{pmatrix} -1 & 0 & 0 \\ 0 & -1 & 0 \\ 0 & 0 & 1 \end{pmatrix}$	$O^2 = \begin{pmatrix} -0.9994 & 0.0001 & 0.0340 \\ 0.0001 & -1 & 0.0070 \\ 0.0340 & 0.0070 & 0.9994 \end{pmatrix}$	0.0347	0.9946°	
$o^3 = \begin{pmatrix} 0 & 1 & 0 \\ -1 & 0 & 0 \\ 0 & 0 & 1 \end{pmatrix}$	$O^3 = \begin{pmatrix} 0.0003 & 0.9999 & 0.0135 \\ -0.9998 & 0 & 0.0205 \\ 0.0205 & -0.0135 & 0.9997 \end{pmatrix}$	0.0245	0.9946°	
$r = \begin{pmatrix} -1 & 0 & 0 \\ 0 & 1 & 0 \\ 0 & 0 & 1 \end{pmatrix}$	$R = \begin{pmatrix} -0.9994 & 0.0315 & 0.0126 \\ 0.0315 & 0.9995 & -0.0002 \\ 0.0126 & -0.0002 & 0.9999 \end{pmatrix}$	0.0339	0.9713°	
$ro = \begin{pmatrix} 0 & 1 & 0 \\ 1 & 0 & 0 \\ 0 & 0 & 1 \end{pmatrix}$	$RO = \begin{pmatrix} 0.0315 & 0.9994 & 0.0126 \\ 0.9995 & -0.0315 & -0.0002 \\ -0.0002 & -0.0126 & 0.9999 \end{pmatrix}$	0.0339	0.9373°	
$ro^2 = \begin{pmatrix} 1 & 0 & 0 \\ 0 & -1 & 0 \\ 0 & 0 & 1 \end{pmatrix}$	$RO^2 = \begin{pmatrix} 0.9994 & -0.0315 & 0.0126 \\ -0.0315 & -0.9995 & -0.0002 \\ -0.0126 & 0.0002 & 0.9999 \end{pmatrix}$	0.0339	0.9020°	
$ro^3 = \begin{pmatrix} 0 & -1 & 0 \\ -1 & 0 & 0 \\ 0 & 0 & 1 \end{pmatrix}$	$RO^3 = \begin{pmatrix} -0.0315 & -0.9994 & 0.0126 \\ -0.9995 & 0.0315 & -0.0002 \\ 0.0002 & 0.0126 & 0.9999 \end{pmatrix}$	0.0339	0.9373°	

Table 2 Detected symmetries of a arrow



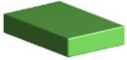
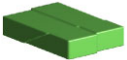
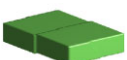
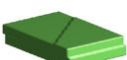

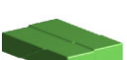


(a) Known symmetry K	(b) Detected symmetry D	(c) $\ K - D\ $	(d) $ \epsilon $	(e) $\Lambda(D)B$
$E = \begin{pmatrix} 1 & 0 & 0 \\ 0 & 1 & 0 \\ 0 & 0 & 1 \end{pmatrix}$	$E = \begin{pmatrix} 1 & 0 & 0 \\ 0 & 1 & 0 \\ 0 & 0 & 1 \end{pmatrix}$	0	0	
$R_{\bar{x}} = \begin{pmatrix} -1 & 0 & 0 \\ 0 & 1 & 0 \\ 0 & 0 & 1 \end{pmatrix}$	$R_{\bar{g}} = \begin{pmatrix} -0.9997 & 0 & 0.0264 \\ 0 & 1 & 0 \\ 0.0264 & 0 & 0.9997 \end{pmatrix}$	0.0264	0.7561°	

Table 3 Detected symmetries of the box

(a) Known symmetry K	(b) Detected symmetry D	(c) $\ K - D\ $	(d) $ \epsilon $	(e) $\Lambda(D)B$
$E = \begin{pmatrix} 1 & 0 & 0 \\ 0 & 1 & 0 \\ 0 & 0 & 1 \end{pmatrix}$	$E = \begin{pmatrix} 1 & 0 & 0 \\ 0 & 1 & 0 \\ 0 & 0 & 1 \end{pmatrix}$	0	0	
$o_1 = \begin{pmatrix} 1 & 0 & 0 \\ 0 & -1 & 0 \\ 0 & 0 & -1 \end{pmatrix}$	$O_1 = \begin{pmatrix} 0.9999 & 0.0112 & 0.0126 \\ 0.0112 & -0.9999 & 0.0001 \\ 0.0126 & 0.0001 & -0.9999 \end{pmatrix}$	0.0169	0.4835°	
$o_2 = \begin{pmatrix} -1 & 0 & 0 \\ 0 & 1 & 0 \\ 0 & 0 & -1 \end{pmatrix}$	$O_2 = \begin{pmatrix} -0.9996 & -0.0288 & 0.0001 \\ -0.0288 & 0.9995 & -0.0094 \\ 0.0001 & -0.0094 & -1 \end{pmatrix}$	0.0303	0.8681°	
$o_3 = \begin{pmatrix} -1 & 0 & 0 \\ 0 & -1 & 0 \\ 0 & 0 & 1 \end{pmatrix}$	$O_3 = \begin{pmatrix} -1 & -0.0001 & -0.0097 \\ -0.0001 & -0.9999 & 0.0115 \\ -0.0097 & 0.0115 & 0.9999 \end{pmatrix}$	0.0151	0.4319°	
$I = \begin{pmatrix} -1 & 0 & 0 \\ 0 & -1 & 0 \\ 0 & 0 & -1 \end{pmatrix}$	$I = \begin{pmatrix} -1 & 0 & 0 \\ 0 & -1 & 0 \\ 0 & 0 & -1 \end{pmatrix}$	0	0	
$Io_1 = \begin{pmatrix} -1 & 0 & 0 \\ 0 & 1 & 0 \\ 0 & 0 & 1 \end{pmatrix}$	$IO_1 = \begin{pmatrix} -0.9999 & -0.0112 & -0.0126 \\ -0.0112 & 0.9999 & -0.0001 \\ -0.0126 & -0.0001 & 0.9999 \end{pmatrix}$	0.0169	0.4835°	
$Io_2 = \begin{pmatrix} 1 & 0 & 0 \\ 0 & -1 & 0 \\ 0 & 0 & 1 \end{pmatrix}$	$IO_2 = \begin{pmatrix} 0.9996 & 0.0288 & -0.0001 \\ 0.0288 & -0.9995 & 0.0094 \\ -0.0001 & 0.0094 & 1 \end{pmatrix}$	0.0303	0.8681°	
$Io_3 = \begin{pmatrix} 1 & 0 & 0 \\ 0 & 1 & 0 \\ 0 & 0 & -1 \end{pmatrix}$	$IO_3 = \begin{pmatrix} 1 & 0.0001 & 0.0097 \\ 0.0001 & 0.9999 & -0.0115 \\ 0.0097 & -0.0115 & -0.9999 \end{pmatrix}$	0.0151	0.4319°	

i.e., the elements of \mathcal{G}_B , in matrix representation. Column (b) describes the detected elements of \mathcal{G}_B in matrix representation. Column (c) is the SVD distance between the known and the detected symmetries, which is the maximal singular value of the difference matrix. Column (d) describes only rotations and reflections. $\epsilon = \angle(\vec{a}, \vec{d})$, where \vec{a} is the actual axis and \vec{d} is the detected

one. Column (e) is $\Lambda(D)B$, where D is the detected isometry.

In particular, Tables 4–6 report the results of analyzing real medical volumes, where Table 5 depicts the results of analyzing a noisy medical volume. In all cases, the proposed scheme was able to recover the underlying volumetric symmetries.

Table 4 Detected symmetries of the skull mode

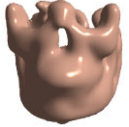
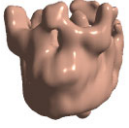
(a) Known symmetry K	(b) Detected symmetry D	(c) $\ K - D\ $	(d) $ \epsilon $	(e) $\Lambda(D)B$
$E = \begin{pmatrix} 1 & 0 & 0 \\ 0 & 1 & 0 \\ 0 & 0 & 1 \end{pmatrix}$	$E = \begin{pmatrix} 1 & 0 & 0 \\ 0 & 1 & 0 \\ 0 & 0 & 1 \end{pmatrix}$	0	0	
$R_{\vec{a}} = \begin{pmatrix} -1 & 0 & 0 \\ 0 & 1 & 0 \\ 0 & 0 & 1 \end{pmatrix}$	$R_{\vec{a}} = \begin{pmatrix} -0.9175 & 0.2354 & -0.0294 \\ 0.2354 & 0.9719 & 0.0035 \\ -0.0294 & 0.0035 & 0.9996 \end{pmatrix}$	0.2389	6.8615°	

Table 5 Detected symmetries of the noisy head model

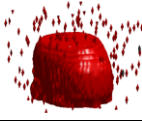


(a) Known symmetry K	(b) Detected symmetry D	(c) $\ K - D\ $	(d) $ \epsilon $	(e) $\Lambda(D)B$
$E = \begin{pmatrix} 1 & 0 & 0 \\ 0 & 1 & 0 \\ 0 & 0 & 1 \end{pmatrix}$	$E = \begin{pmatrix} 1 & 0 & 0 \\ 0 & 1 & 0 \\ 0 & 0 & 1 \end{pmatrix}$	0	0	
$R_{\vec{a}} = \begin{pmatrix} -1 & 0 & 0 \\ 0 & 1 & 0 \\ 0 & 0 & 1 \end{pmatrix}$	$R = \begin{pmatrix} -0.8986 & -0.0427 & -0.4367 \\ -0.0427 & 0.9990 & -0.0098 \\ -0.4367 & -0.0098 & 0.8996 \end{pmatrix}$	0.4503	13.0178°	

Table 6 Detected symmetries of the bone model

(a) Known symmetry K	(b) Detected symmetry D	(c) $\ K - D\ $	(d) $ \epsilon $	(e) $\Lambda(D)B$
$E = \begin{pmatrix} 1 & 0 & 0 \\ 0 & 1 & 0 \\ 0 & 0 & 1 \end{pmatrix}$	$E = \begin{pmatrix} 1 & 0 & 0 \\ 0 & 1 & 0 \\ 0 & 0 & 1 \end{pmatrix}$	0	0	

6 Conclusions

In this work, we proposed a novel approach for detecting and analyzing symmetries in 3D volumes. We utilized the invariance of symmetries with respect to the Fourier transform and applied the pseudo-polar Fourier transform to represent the volume in a pseudo-polar Fourier representation. This allowed to accurately compute the ADF of the input volume and its rotated/inverted replica. Thus, we recovered the rotational symmetries group of the volume. In our second contribution, we derived a novel group theory based rigorous analysis of 3D symmetries. This paved the way to recover the entire set of symmetries (including the inverted-rotational symmetries) given the recovered rotational ones. We applied our approach to real as well as synthetic volumes. The results and showed them to be accurate and robust to the presence of imperfect symmetries and noise that are common in real volumes.

References

- Averbuch, A., & Shkolnisky, Y. (2003). 3D Fourier based discrete radon transform. *Applied and Computational Harmonic Analysis*, 15, 33–69.
- Bokeloh, M., Berner, A., Wand, M., Seidel, H.-P., & Schilling, A. (2009). Symmetry detection using line features. *Computer Graphics Forum (Proc. EUROGRAPHICS)*, 28(2), 697–706.
- Bronstein, A. M., Bronstein, M. M., & Kimmel, R. (2006). Generalized multidimensional scaling: a framework for isometry-invariant partial surface matching. *Proceedings of the National Academy of Science*, 103(5), 1168–1172.
- Bronstein, M. M., Raviv, D., Bronstein, A. M., & Kimmel, R. (2009). Full and partial symmetries of non-rigid shapes. *IJCV*.
- Chen, S. (2001). Extraction of local mirror-symmetric feature by odd-even decomposition. *Proceedings International Conference on Image Processing*, 3, 756–759.
- Chertok, M., & Keller, Y. (2009). Spectral symmetry analysis. *IEEE Transactions on Pattern Analysis and Machine Intelligence* (in press). <http://doi.ieeeecomputersociety.org/10.1109/TPAMI.2009.121>.
- Cheung, W., & Hamarneh, G. (2007). *N*-sift: *N*-dimensional scale invariant feature transform for matching medical images. In *4th*

- IEEE international symposium on biomedical imaging: from nano to macro, 2007. ISBI 2007* (pp. 720–723).
- Cornelius, H., Perdoch, M., Matas, J., & Loy, G. (2007). Efficient symmetry detection using local affine frames. In B. K. Ersbøll, & K. S. Pedersen (Eds.), *SCIA 2007: Proceedings of 15th Scandinavian conference on image analysis. Lecture notes in computer science* (Vol. 4522, pp. 152–161). Berlin: Springer.
- Derrode, S., & Ghorbel, F. (2004). Shape analysis and symmetry detection in gray-level objects using the analytical Fourier-Mellin representation. *Signal Processing*, 84(1), 25–39.
- Eckmann Jeger, B., & Jeger, M. (1967). *Vector geometry & linear algebra*. New York: John Wiley & Sons.
- Hays, J. H., Leordeanu, M., Efros, A. A., & Liu, Y. (2006). Discovering texture regularity via higher-order matching. In *9th European conference on computer vision* (pp. 522–535).
- Holden, A. (1971). *Shapes, space and symmetry*. New York: Columbia University Press.
- Kazhdan, M. M., Chazelle, B., Dobkin, D. P., Finkelstein, A., & Funkhouser, T. A. (2002). A reflective symmetry descriptor. In *ECCV '02: Proceedings of the 7th European conference on computer vision-part II* (pp. 642–656). Berlin: Springer-Verlag.
- Keller, Y., & Shkolnisky, Y. (2006). A signal processing approach to symmetry detection. *IEEE Transactions on Image Processing*, 15(6), 2198–2207.
- Keller, Y., Averbuch, A., & Israeli, M. (2005a). Pseudo-polar based estimation of large translations rotations and scalings in images. *IEEE Transactions on Image Processing*, 14(1), 12–22.
- Keller, Y., Shkolnisky, Y., & Averbuch, A. (2005b). The angular difference function and its application to image registration. *IEEE Transactions on Pattern Analysis and Machine Intelligence*, 27(6), 969–976.
- Keller, Y., Shkolnisky, Y., & Averbuch, A. (2006). Algebraically accurate 3-D rigid registration. *IEEE Transactions on Signal Processing*, 54(11), 4323–4331.
- Kim, W., & Kim, Y. (1999). Robust rotation angle estimator. *IEEE Transactions on Pattern Analysis and Machine Intelligence*, 21(8), 768–773.
- Kiryati, N., & Gofman, Y. (1998). Detecting symmetry in grey level images: the global optimization approach. *International Journal of Computer Vision*, 29(1), 29–45.
- Lowe, D. (2003). Distinctive image features from scale-invariant keypoints. *International Journal of Computer Vision*, 20, 91–110.
- Loy, G., & Eklundh, J.-O. (2006). Detecting symmetry and symmetric constellations of features. In *Proc. European conf. comp. vision (ECCV'06). LNCS* (Vol. 3951, pp. 508–521). Berlin: Springer.
- Lucchese, L. (2004). Frequency domain classification of cyclic and dihedral symmetries of finite 2-D patterns. *Pattern Recognition*, 37, 2263–2280.
- Martinet, A., Soler, C., Holzschuch, N., & Sillion, F. (2006). Accurate detection of symmetries in 3d shapes. *ACM Transactions on Graphics*, 25(2), 439–464.
- Miller, W. (1972). *Symmetry groups and their applications*. London: Academic Press.
- Mitra, N. J., Guibas, L., & Pauly, M. (2006). Partial and approximate symmetry detection for 3D geometry. *ACM Transactions on Graphics*, 25, 560–568.
- Ni, D., Chui, Y. P., Qu, Y., Yang, X., Qin, J., Wong, T.-T., Ho, S. S. H., & Heng, P. A. (2009). Reconstruction of volumetric ultrasound panorama based on improved 3D sift. *Computerized Medical Imaging and Graphics*, 33(7), 559–566.
- Ovsjanikov, M., Sun, J., & Guibas, L. J. (2008). Global intrinsic symmetries of shapes. *Computer Graphics Forum*, 27(5), 1341–1348.
- Pauly, M., Mitra, N. J., Wallner, J., Pottmann, H., & Guibas, L. (2008). Discovering structural regularity in 3D geometry. *ACM Transactions on Graphics*, 27(3):1–11. 43.
- Prasad, V. S. N., & Davis, L. S. (2005). Detecting rotational symmetries. In *Tenth IEEE international conference on computer vision, 2005. ICCV 2005* (Vol. 2, pp. 954–961), 17–21 Oct. 2005.
- Prasad, V. S. N., & Yegnanarayana, B. (2004). Finding axes of symmetry from potential fields. *IEEE Transactions on Image Processing*, 13(12), 1559–1566.
- Raviv, D., Bronstein, A. M., Bronstein, M. M., & Kimmel, R. (2007). Symmetries of non-rigid shapes. In *IEEE 11th international conference on computer vision, 2007. ICCV 2007* (pp. 1–7).
- Reisfeld, D., Wolfson, H., & Yeshurun, Y. (1995). Context free attentional operators: the generalized symmetry transform. *International Journal of Computer Vision*, 14, 119–130.
- Shen, D., Ip, H., & Teoh, E. K. (2001). Robust detection of skewed symmetries by combining local and semi-local affine invariants. *Pattern Recognition*, 34(7), 1417–1428.
- Stoy, G. A., Neumann, P. M., & Thompson, E. C. (1994). *Groups and geometry*. Oxford: Oxford University Press.
- Thompson, D. W. (1961). *On growth and form*. Cambridge University Press, Cambridge.
- Trucco, E., & Verri, A. (1998). *Introductory techniques for 3-D computer vision*. New Jersey: Prentice-Hall (pp. 333–334).
- Weyl, H. (1952). *Symmetry*. Princeton: Princeton University Press.